Design and Development of RIS-assisted Systems for sub-6 GHz Operations

M.Tech. Thesis

by
SUMIT GAURAV



DEPARTMENT OF ELECTRICAL ENGINEERING
INDIAN INSTITUTE OF TECHNOLOGY INDORE
May, 2026

Design and Development of RIS-assisted Systems for sub-6 GHz Operations

A THESIS

Submitted in partial fulfillment of the requirements for the award of the degree
of
Master of Technology

by
SUMIT GAURAV



DEPARTMENT OF ELECTRICAL ENGINEERING
INDIAN INSTITUTE OF TECHNOLOGY INDORE
May, 2026

INDIAN INSTITUTE OF TECHNOLOGY INDORE

CANDIDATE'S DECLARATION

I hereby certify that the work which is being presented in the thesis entitled "**Design and Development of RIS-assisted Systems for sub-6 GHz Operations**" in the partial fulfillment of the requirements for the award of the degree of Master of Technology and submitted in the Department of Electrical Engineering, Indian Institute of Technology Indore, is an authentic record of my own work carried out during the time period from July, 2024 to May, 2026 under the supervision of Dr. Saptarshi Ghosh, Indian Institute of Technology, Indore, India.

The matter presented in this thesis has not been submitted by me for the award of any other degree of this or any other institute.

Sumit 11/05/26

Signature of the student with Date

(Sumit Gaurav)

This is to certify that the above statement made by the candidate is correct to the best of my knowledge.

Saptarshi Ghosh 11-05-26

Signature of Supervisor of M.Tech. Thesis with Date

(Dr. Saptarshi Ghosh)

Sumit Gaurav has successfully given his M.Tech. Oral Examination held on **27/04/2026.**

Saptarshi Ghosh 11-05-26

Signature of Supervisor of M.Tech. Thesis with Date

(Dr. Saptarshi Ghosh)

Saptarshi Ghosh 11-05-26

Signature of Convenor, DPGC with Date

(Dr. Saptarshi Ghosh)

Acknowledgements

My journey through the M.Tech. program has been both challenging and rewarding, shaped greatly by the guidance and support of many individuals. Looking back, choosing Dr. Saptarshi Ghosh as my supervisor was one of the most valuable decisions of my academic journey. What began as a formal academic association gradually evolved into a meaningful mentorship. His constant encouragement, insightful feedback, and unwavering support not only improved the quality of my research but also helped me grow as a researcher and individual. Our technical discussions often pushed me to think more critically and explore ideas more deeply. Beyond his academic brilliance, his humility and personal qualities have left a lasting impression on me.

I sincerely thank Dr. Dibbendu Roy, Dr. Ayush Tripathi, Dr. Appina Balasubramaniam, and Dr. Vivek Kanhangad, the members of my Research Progress Committee, for evaluating my work throughout the semesters. Their valuable suggestions and constructive feedback helped improve this research significantly. I am also grateful to Dr. Swaminathan R., Head of the Department of Electrical Engineering, for his support and encouragement during my MTech program.

I express my heartfelt gratitude to my Ph.D. project guide, Mr. P. Megh Sainadh, whose guidance and support were crucial for the completion of this work. His patience in explaining concepts, willingness to clarify even the smallest doubts, and continuous motivation helped me overcome several technical challenges. I am especially thankful for encouraging me to step out of my comfort zone and explore new ideas with confidence.

I would also like to thank my colleagues and lab mates, especially Mr. Akhila Gouda, Mr. Soham Nandi, and Dr. Poonam Tiwari, for their constant support and guidance. The collaborative environment and shared discussions made this journey more enriching and enjoyable. I am equally thankful to my dear friends Ms.

Aishwarya Gupta, Mr. Deepak Kaushik, Mr. Munna Aziz, and Mr. Deepak Solanki for their encouragement, positivity, and companionship throughout this journey.

I also acknowledge my fellow M.Tech. seniors for fostering a collaborative learning environment and making this experience intellectually stimulating. I am equally thankful to the B.Tech. students I interacted with and guided, whose enthusiasm and support also contributed to my learning experience.

I deeply appreciate my school, college, and undergraduate friends who have remained close to me over the years, offering encouragement and support through every phase of life. I am thankful to all the institutions and teachers who shaped my academic journey, especially during my undergraduate studies at the National Institute of Technology, Rourkela, which laid the foundation for this work.

Finally, I express my deepest gratitude to my parents. Their unconditional love, endless patience, sacrifices, and unwavering belief in me have been my greatest strength. They supported me through every challenge and celebrated every small achievement with me. This journey would not have been possible without their constant presence and blessings, and for that, I will always remain forever grateful.

Sumit Gaurav

Dedicated to my loving parents,

who have supported me throughout

this journey.

Abstract

Reconfigurable Intelligent Surfaces (RIS) have emerged as a promising technology for next-generation wireless communication and electromagnetic wave manipulation, offering low-cost, energy-efficient, and highly adaptable alternatives to conventional systems. This thesis presents a comprehensive study on the design, analysis, and development of metasurface-based RIS architectures, progressing from passive digitally coded metasurfaces (DCMS) to advanced reconfigurable and multifunctional structures. The primary objective of this work is to overcome the limitations of conventional metasurfaces, such as fixed functionality, limited beam control, and lack of adaptability, while enabling efficient beam steering, multi-beam generation, and additional functionalities such as simultaneous wireless information and power transfer (SWIPT) and radar cross-section (RCS) reduction.

The research begins with the development of a passive DCMS operating at 5 GHz, where discrete phase coding is utilized to achieve controlled wavefront manipulation. By employing a 3-bit coding scheme, the metasurface demonstrates single, dual, and quad beam steering capabilities, enabling multi-directional coverage suitable for multi-user communication scenarios. The phase synthesis based on generalized Snell's law allows accurate beam steering with improved radiation characteristics and reduced sidelobe levels. While the passive design provides low complexity and energy-efficient operation, its major limitation lies in the fixed phase distribution after fabrication, restricting its adaptability in dynamic environments .

To extend the applicability of passive metasurfaces, a second DCMS design operating at 2.5 GHz is proposed, focusing on SWIPT-enabled IoT applications. At lower frequencies, larger wavelengths allow the realization of electrically larger apertures, enhancing interaction with incident waves. The proposed structure demonstrates efficient single and multi-beam steering along with energy focusing capabilities. By redirecting electromagnetic waves toward specific spatial

locations, the metasurface enables simultaneous delivery of information and power to energy-constrained IoT devices, particularly in non-line-of-sight (NLOS) environments. This approach improves communication reliability and energy harvesting efficiency, making it suitable for applications such as smart agriculture, wireless sensor networks, and battery-free IoT systems .

To address the inherent limitation of passive structures, the work further advances toward active RIS architectures incorporating electronically tunable components. An individually controlled RIS operating at 5.4 GHz is developed using varactor diodes, enabling real-time control of the reflection phase. The design evolves from column-wise biasing to fully independent biasing of each unit cell, significantly increasing the degrees of freedom in phase manipulation. This enables dynamic beam steering, dual-beam generation, and flexible power allocation among multiple users. The proposed structure demonstrates robust performance under both normal and oblique incidence conditions, validating its suitability for adaptive wireless communication systems and multi-user environments .

Finally, the thesis introduces a switchable RIS operating at 3.5 GHz, integrating both reflection and absorption functionalities within a single platform. By incorporating p-i-n diodes for switching and varactor diodes for phase tuning, the metasurface can dynamically transition between RIS mode and absorber mode. In the reflective state, it enables programmable beam steering, while in the absorptive state, it suppresses reflections by dissipating incident electromagnetic energy. This dual functionality is particularly relevant for defense applications, where communication and stealth must coexist, as well as for advanced wireless systems requiring interference suppression and energy-efficient operation .

Overall, this thesis demonstrates a systematic progression from passive to active and from single-function to multifunctional RIS architectures. The proposed designs provide scalable, low-cost, and efficient solutions for adaptive electromagnetic control, with potential applications in 5G/6G communication

systems, IoT networks, smart environments, radar systems, and defense technologies. The outcomes of this research establish a strong foundation for future development of intelligent, programmable metasurfaces capable of real-time environmental interaction and autonomous operation.

TABLE OF CONTENTS

List of Figures xvii
List of Tables xxiii
List of Abbreviations/Acronyms xxv
List of Symbols xxvii

1 Introduction 1

1.1 Reconfigurable Intelligent Surfaces (RIS) – An Overview 2

1.2 RIS Functionalities & Applications 3

1.2.1 Elementary Functions of RIS 3
1.2.2 Applications of RIS 5

1.3 Literature Survey on RIS Geometry 6

1.3.1 Phase Distribution Synthesis for Beam Steering 7
1.3.2 Passive DCMS for Single-Beam Steering 9
1.3.3 Active DCMS or RIS for Beam Steering 11
1.3.4 Switchable RIS Geometry Exhibiting Multifunctional Responses 17

1.4 Problem Statement 20

1.5 Organization of the Thesis 21

2 Passive DCMS for Multi-Beam Steering 23

2.1 Introduction 23

2.2 Unit Cell Geometry 24

2.3 Generalized Snell's Law 25

2.4 Single-Beam Steering Operation 27

2.4.1 Normal Incidence 27
2.4.2 Oblique Incidence 28
2.5 Multi-Beam Steering Operation 30
2.5.1 Dual-Beam Steering 30
2.5.2 Quad-Beam Steering 32
2.6 Conclusion 33

3 Passive DCMS for Beam Steering and SWIPT 35
3.1 Introduction 35
3.2 Unit Cell Geometry 35
3.3 Beam Steering Operation 37
3.3.1 Single-Beam Steering 38
3.3.2 Dual-Beam Steering 39
3.4 SWIPT Enabled IoT Application 40
3.5 Conclusion 42

4 Dynamically - Controlled RIS Geometry 45
4.1 Introduction 45
4.2 Working Principle of Electronic Diodes 46
4.3 RIS Geometry with Reduced Control Network 47
4.3.1 Unit Cell Geometry 48
4.3.2 Beam Steering Operation 50
4.4 Individually Controlled RIS Geometry 51
4.4.1 Unit Cell Geometry 52
4.5 Beam Steering Operation 54
4.5.1 Single-Beam Steering 55
4.5.2 Dual-Beam Steering 56

4.6 Conclusion 58

5 Switchable RIS for Dual Functionality 61

5.1 Introduction 61

5.2 Reflection and Absorption Mechanism 61

5.3 Unit Cell Geometry 63

5.4 Biasing of Electronic Components 65

5.5 Beam Steering Operation (OFF State) 66

5.5.1 Single-Beam Steering 67

5.5.2 Dual-Beam Steering 69

5.6 Absorption Mechanism & RCS Reduction (ON State) 70

5.7 Conclusion 72

6 Conclusion & Future Scope 75

6.1 Summary of the Research 75

6.2 Scope of Future Work 79

References xxix

List of Publications xxxiii

LIST OF FIGURES

1.1 Illustration of fundamental RIS functionalities for electromagnetic wave manipulation [Ref. (6)] 4

1.2 Overview of RIS-assisted communication scenarios and SWIPT-enabled IoT applications. [Ref. (6)] 5

1.3 (i) Illustration of beam steering using coded reflective metasurface. (ii) Systematic design flowchart for digitally coded reflective metasurface design to achieve the desired reflection angle under the illumination of a normal incidence plane wave. [Ref. (8)] 8

1.4 (i) Unit cell geometry for 1-bit coding (a) element 0 and (b) element 1; for 2-bit coding (c) element 00, (d) element 01, (e) element 10, and (f) element 11 (Dimensions: W_0 =8.2 mm, W_1 =7.15 mm, W_{00} =8.45 mm, W_{01} =6.6 mm, W_{10} =7.3 mm, W_{11} =7.75 mm, and a = $\lambda_0/6$). (ii) Variation of phase and magnitude response with frequency for the unit cell elements of for 2-bit coding. [Ref. (8)] 10

1.5 Normalized radiation pattern of coded metasurface design in CST with a size of $10\lambda_0 \times 10\lambda_0$ showing a reflected beam direction of ($\theta r = 30^\circ, \varphi r = 0^\circ$) for (i) 1-bit coding with SLL–7.6 dB and (ii) 2-bit coding with SLL–12.18 dB. The incident wave is normal to the metasurface. [Ref. (8)] 11

1.6 Sketch of the proposed meta-atom, in which a varactor is embedded to tune the reflection phase. The metallic vias are employed to reduce the mutual coupling between adjacent meta-atoms and improve the angular insensitivity. (i) Explosive view, (ii) top view and (iii) side view of the meta-atom. [Ref. (17)] 12

1.7 Numerical simulation results for the (i) amplitudes and (ii) phase responses of the proposed RIS at normal incidence. [Ref. (17)] 13

1.8 Simulated RIS scattering patterns at incident angles θ_i of (i) 112.5°, (ii) 150°, (iii) Normalized 2D scattering beam patterns at incident angles of 90°, 122.5°, 150°, and 122°. The RIS angular reciprocity can be obtained from the angle-insensitive meta-atom. [Ref. (17)] 14

1.9 Geometry of the proposed 3-bit mm-wave RIS unit cell. (i) Front view. (ii) Top view. [Ref. (18)] 15

1.10 Reflection coefficients for different operating states. (i) Amplitude. (ii) Phase. Ten curves for different capacitance values are shown, eight of which are identified as

the used states (separated by 45° phase interval at 28 GHz), and the other two are the upper and lower limits. [Ref. (18)] 16

1.11 (i) Quantized phase distribution of the RIS for 30° beam pointing. (ii) Radiation pattern at 28 GHz in φ = 0 plane, inset is the 3D pattern. [Ref. (18)] 16

1.12 Illustration of a Switchable RIS which transforms incoming incident fields into desired scattered fields via active unit cells consisting of varactor and p-i-n diodes for an independent phase and amplitude control resp. [Ref. (25)] 17

1.13 (i) Proposed metasurface unit cell architecture based on coupled Split Ring Resonator (SRR) and Dipole Ring Resonator (DRR), loaded with tunable capacitor and resistor respectively. (b) FEM-Simulated magnitude and phase of three configuration (R = 25 Ω and C = 0.1 pF). [Ref. (25)] 18

1.14 (i) Illustration of the simulation setup in FEM-HFSS for a finite size metasurface consisting of N unit cells with N lumped resistors and capacitors. The unit cell array is excited with a normally incident linearly polarized plane wave. (ii) Specified peak reflection with beam deflection to -15◦. Normally incident plane-wave and metasurface consists of 20 cells. [Ref. (25)] 19

2.1 Unit Cell geometry of the proposed digital coded metasurface: (i) top view, (ii) isometric view. The optimized dimensions are as follows: L = 13mm, and h = 1.6mm. (iii) Table 1: Eight coding states of the proposed DCMS. 24

2.2 Simulated S_{11} responses for different patch lengths (p) at 5 GHz: (a) magnitude response, and (b) phase response. 25

2.3 Simulated response of the proposed 1-bit RIS geometry for single beam steering under normal incidence conditions. 27

2.4 Simulated response of the proposed 3-bit RIS geometry for single beam steering under normal incidence conditions. 28

2.5 Simulated response of the proposed 3-bit RIS geometry for single beam steering under oblique incidence conditions. 29

2.6 Simulated response of the proposed 3-bit RIS geometry for single beam steering under oblique incidence conditions. 29

2.7 Simulated response of the proposed 3-bit RIS geometry for dual beam steering under normal incidence conditions and with equal power distribution. 31

2.8 Simulated response of the proposed 3-bit RIS geometry for dual beam steering under normal incidence conditions and with unequal power distribution. 31

2.9 Simulated response of the proposed 3-bit RIS geometry for quad beam steering under normal incidence conditions and with equal power distribution. 32

3.1 Unit cell geometry of the proposed digital coded metasurface: (i) top view, (ii) isometric view. The optimized dimensions are as follows: L = 10 mm, and h = 4.8 mm. (iii) Table 2: Eight coding states of the proposed DCMS. 36

3.2 Simulated S_{11} responses for different patch lengths (k) and (m) at 2.5 GHz: (i) magnitude response, and (ii) phase response. 37

3.3 Simulated response of the proposed 2-bit RIS geometry for single beam steering under normal incidence conditions. 37

3.4 Simulated response of the proposed 3-bit RIS geometry for single beam steering under normal incidence conditions. 38

3.5 Simulated response of the proposed 3-bit RIS geometry for single beam steering under oblique incidence conditions. 38

3.6 Simulated response of the proposed 3-bit RIS geometry for dual beam steering under normal incidence conditions and with equal power distribution. 39

3.7 Simulated response of the proposed 3-bit RIS geometry for dual beam steering under normal incidence conditions and with unequal power distribution. 40

3.8 Illustration of the proposed RIS-assisted SWIPT system for IoT in NLOS conditions using Snell's law-based beam steering. 41

4.1 Comparison of passive DCMS and active RIS architecture (i) Passive DCMS geometry with fixed beam steering (no intelligence), (ii) Active RIS geometry with programmable beam control enabling multi-user support (intelligence). 45

4.2 Equivalent circuit models of p-i-n diode in the ON and OFF states and varactor diode illustrating voltage-controlled junction capacitance. 46

4.3 Unit cell geometry of proposed RIS. (i) Top view. (ii) Side view. (iii) Isometric view. The geometric dimensions of the square unit cell are: L = 11mm, P = 10.7 mm, q = 10.8 mm, h_1 = 1.6 mm, h_2 = 0.8 mm, and th = 0.2 mm. 48

4.4 Simulated S_{11} responses of the proposed unit cell geometry at four coding states: (i) Magnitude, and (ii) phase states of the proposed RIS with and without air spacer. 49

4.5 Simulated response of the proposed 2-bit RIS geometry for single beam steering under normal incidence conditions. 50

4.6 Simulated response of the proposed 2-bit RIS geometry for dual beam steering under normal incidence conditions. 51

4.7 Unit cell geometry of proposed RIS. (i) Top view. (ii) Side view. (iii) Isometric view. The geometric dimensions of the square unit cell are: L = 7.5mm, q = 7.3mm, p = 7.3mm, r = 4mm, s = 0.5mm, h_1 = 2mm, h_2 = 1.2mm, th = 0.1mm. 52

4.8 Simulated S_{11} responses of the proposed unit cell geometry at four coding states: (i) Phase, and (ii) Magnitude response of the proposed RIS. 53

4.9 Simulated response of the proposed 1-bit RIS geometry for single beam steering under normal incidence conditions. 55

4.10 Simulated response of the proposed 2-bit RIS geometry for single beam steering under normal incidence conditions. 56

4.11 Simulated response of the proposed 2-bit RIS geometry for single beam steering under oblique incidence conditions. 56

4.12 Simulated response of the proposed 2-bit RIS geometry for dual beam steering under normal incidence conditions with unequal power distribution. 57

4.13 Simulated response of the proposed 2-bit RIS geometry for dual beam steering under normal incidence conditions with unequal power distribution. 58

5.1 Schematic representation of the proposed switchable metasurface: (i) RIS reflection for beam steering, (ii) microwave absorber. 62

5.2 Unit cell geometry of the proposed switchable metasurface: (i) Top view, (ii) isometric view, (iii) side view, (iv) ground plane, and (v) biasing layer. The optimized dimensions are as follows: a = 10 mm, b = 4.3 mm, b_1 = 3.2 mm, c = 0.2 mm, c_1 = 0.1 mm, h_1 = 3.6mm, h_2 = 1.0mm. 63

5.3 Simulation S_{11} response of the proposed switchable metasurfaces under different switching modes. OFF state: (i) magnitude, (ii) phase, ON state: (iii) magnitude. 64

5.4 Illustration of the biasing present in the proposed switchable metasurface. 66

5.5 Simulated response of the proposed 1-bit RIS geometry for single beam steering under normal incidence conditions. 67

5.6 Simulated response of the proposed 2-bit RIS geometry for single beam steering under normal incidence conditions. 68

5.7 Simulated response of the proposed 2-bit RIS geometry for single beam steering under oblique incidence conditions. 68

5.8 Simulated response of the proposed 2-bit RIS geometry for dual beam steering under normal incidence conditions with equal power distribution. 69

5.9 Normalized absorption response of the proposed switchable metasurface for different capacitance values: (i) OFF state RIS operation at 3.5GHz, (ii) ON state absorption operation at 2.4GHz. 70

6.1 Evolution from Passive to Electronically Active RIS and Proposed Intelligent Control Architecture for a 32x32 element RIS. 80

6.2 Schematic of the proposed RIS control board circuit illustrating Shift Register based Digital Input, MUX for Voltage selection, and PMOS based RF-Isolated Biasing Network. 81

LIST OF TABLES

2.1 Eight coding states of the proposed DCMS. 24

3.1 Eight coding states of the proposed DCMS. 36

4.1 Four coding states of the proposed Individually biased RIS. 53

5.1 Four coding states of the proposed Switchable RIS (OFF State). 64

6.1 Comparative overview of the proposed metasurface unit cells across different design stages highlighting unit cells dimensions, operating frequency, biasing capability, beam steering range, and design methodology. 77

6.2 Performance comparison of the proposed RIS unit cells with reported literature, including unit cell geometry, magnitude and phase responses, and highlighting the novelty of low-cost FR4-based designs. 78

LIST OF ABBREVIATIONS/ACRONYMS

Abbreviation	Full Form
ADC	Analog-to-Digital Converter
CST	Computer Simulation Technology (Microwave Studio)
DC	Direct Current
DCMS	Digitally Coded Metasurface
DRR	Dipole Ring Resonator
EM	Electromagnetic
FEM	Finite Element Method
FEBI	Finite Element Boundary Integral
FR4	Flame Retardant 4 (Dielectric Substrate Material)
HFSS	High Frequency Structure Simulator
IoT	Internet of Things
ISAC	Integrated Sensing and Communication
LOS	Line-of-Sight
MIMO	Multiple Input Multiple Output
mm Wave	Millimeter Wave
NLOS	Non-Line-of-Sight
PCB	Printed Circuit Board
PGMS	Phase Gradient Metasurface
PIN	Positive-Intrinsic-Negative (Diode)
RCS	Radar Cross Section
RF	Radio Frequency
RFID	Radio Frequency Identification
RIS	Reconfigurable Intelligent Surface

RLC	Resistor-Inductor-Capacitor
SIW	Substrate Integrated Waveguide
SRR	Split Ring Resonator
SWIPT	Simultaneous Wireless Information and Power Transfer
THz	Terahertz
TE	Transverse Electric
TM	Transverse Magnetic
SLL	Side Lobe Level

LIST OF SYMBOLS

Symbol	Description
$\Delta\varphi$	Phase shift introduced by RIS unit cell
θ_i	Angle of incidence
φ_i	Azimuth angle of incidence
θ_r	Angle of reflection
φ_r	Azimuth angle of reflection
$\Phi(x,y)$	Spatial phase distribution across metasurface
$d\Phi/dx$, $d\Phi/dy$	Phase gradient along x and y directions
λ_o	Free-space wavelength
k_o	Free-space wave number ($2\pi / \lambda_o$)
k_i, k_r	Incident and reflected wave numbers
Δx, Δy	Unit cell dimensions along x and y axes
L_{cx}, L_{cy}	Cluster dimensions along x and y directions
C_x, C_y	Number of unit cells in cluster
n	Number of coding bits
$B(p,q)$	Coding state matrix
p, q	Indices of unit cells
$\Phi(p,q)$	Phase at discrete unit cell
$F(\theta,\varphi)$	Array factor / radiation pattern
M, N	Number of unit cells along x and y
λ	Wavelength
θ	Observation angle
φ	Azimuth angle
$d\Phi$	Phase difference between adjacent unit cells
x	Spatial coordinate
R	Resistance
L	Inductance / unit cell length (context dependent)

C	Capacitance
ε_r	Relative permittivity
tanδ	Loss tangent
σ	Electrical conductivity
h	Substrate thickness
p	Patch length parameter
k	Wave number
S_{11}	Reflection coefficient
$\Phi_1(x)$, $\Phi_2(x)$, $\Phi_k(x)$	Phase distributions for multi-beam
θ_{r1}, θ_{r2}, θ_{r3}, θ_{r4}	Multiple reflection angles
n_i	Refractive index
dx	Differential distance
$e^{j\Phi(x)}$	Complex exponential phase
arg(.)	Argument of complex number

Chapter 1: Introduction

The exponential growth of wireless communication systems over the past two decades has placed immense pressure on the radio frequency (RF) spectrum, energy resources, and network infrastructure. The global proliferation of smart devices, the emergence of the Internet of Things (IoT), and the ever-increasing demand for high-data-rate, low-latency services have collectively driven the need for innovative and intelligent approaches to wireless network design. Traditional network architectures rely primarily on increasing transmission power, deploying more base stations, or allocating additional spectrum to meet capacity demands - strategies that are reaching their physical, economic, and regulatory limits.

Conventional wireless systems treat the propagation environment as an uncontrollable random entity whose effects - including multipath fading, interference, and signal attenuation - must be mitigated through sophisticated signal processing at the transmitter and receiver ends. This paradigm, while effective to a degree, is inherently reactive: the network adapts to the channel rather than shaping it. The emergence of Reconfigurable Intelligent Surfaces (RIS) represents a fundamental departure from this philosophy, offering the transformative capability to actively engineer the wireless propagation environment itself.

Driven by breakthroughs in metamaterial engineering, microelectromechanical systems, and programmable hardware, RIS technology has rapidly matured from a theoretical concept into a practically realizable solution. It’s potential to enhance spectral efficiency, extend coverage, improve physical layer security, and reduce energy consumption makes it one of the most compelling technologies under investigation for next-generation (6G) wireless networks.

1.1 Reconfigurable Intelligent Surfaces (RIS) – An Overview

RIS are engineered surfaces composed of a large number of sub-wavelength unit cells - commonly referred to as metasurface elements - whose electromagnetic (EM) response, encompassing phase, amplitude, and polarization, can be controlled in a programmable and near-real-time manner. Unlike conventional reflectors or passive scatterers, an RIS possesses the unique ability to dynamically manipulate incident wireless signals by individually tuning the response of each unit cell. By adjusting these unit cells, an RIS can steer, focus, or scatter radio waves in desired directions with a high degree of spatial precision, effectively shaping the wireless channel to meet system-level objectives.

At its physical core, each RIS consists of unit cell, it is a tiny resonant structure - often implemented using p-i-n diodes, varactor diodes, copper patch, and substrates - that introduces a controllable phase shift $\Delta\varphi \in [0, 2\pi]$ to the reflected signal. When a large array of such elements acts in concert under a centralized or distributed controller, the collective phase profile synthesized across the surface creates constructive interference at target locations such as intended receivers, and destructive interference at undesired locations such as eavesdroppers or interference zones. This coherent superposition of reflected wavefronts is the fundamental mechanism through which an RIS enhances signal quality and network performance.

A distinguishing feature of RIS technology is its nearly passive operation. Unlike active relay nodes or massive MIMO base stations, an RIS does not employ power-hungry RF chains, amplifiers, or analog-to-digital converters (ADCs). The energy consumed by an RIS is limited primarily to the low-power control circuitry required to switch or tune the unit cell states. This passive or semi-passive nature renders RIS as an environmentally sustainable and cost-effective solution - particularly attractive for large-scale deployment in dense urban environments, indoor settings, and coverage-challenged areas such as tunnels, stadiums, and industrial facilities. RIS can be physically realized in

multiple forms: planar reflective surfaces mounted on building facades, ceilings, or roadside structures; conformal surfaces wrapped around curved objects and even transparent surfaces integrated into glass windows. The versatility of deployment, combined with the ability to operate across a broad range of frequencies spanning sub-6 GHz, millimeter-wave (mm-wave), and terahertz (THz) bands, positions RIS as a highly adaptable enabling technology for heterogeneous 6G networks.

1.2 RIS functionalities & Applications –

The programmable EM behaviour of RIS enables a rich set of system-level functions and practical applications that extend well beyond simple signal reflection.

1.2.1 Elementary functions of RIS –

The following are the core capabilities that define the role of RIS in modern communication and EM systems.

Reflection: This functionality involves redirecting an incident electromagnetic wave toward a desired direction by introducing a controlled phase variation across the surface. The reflected wave need not follow the conventional law of reflection, enabling anomalous reflection.

Transmission/Refraction: In this case, the metasurface manipulates the transmitted wave by tailoring phase discontinuities across the surface. This allows the refracted wave to propagate in directions not governed by classical Snell's law. By carefully designing the unit cell geometry or incorporating tunable elements, the transmitted wavefront can be dynamically controlled.

Absorption: This function is realized by designing the surface to suppress both reflected and transmitted waves, thereby dissipating the incident electromagnetic energy within the structure. It is typically achieved through impedance matching and the introduction of lossy components, ensuring minimal scattering and maximum energy attenuation.

Focusing/Beamforming: This involves engineering a non-linear phase profile across the metasurface so that the incident wave is concentrated at a specific point or directed along a desired path. By ensuring constructive interference at the target location, the energy of the wave is effectively focused, resulting in enhanced field intensity.

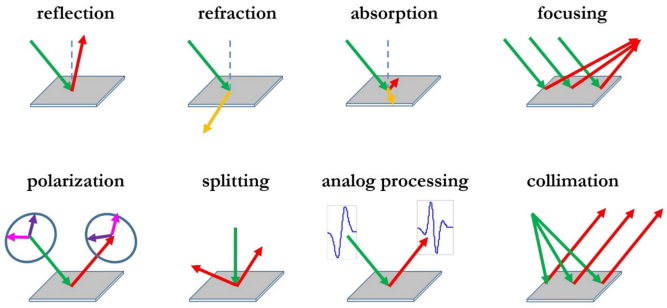

Fig.1.1 Illustration of fundamental RIS functionalities for electromagnetic wave manipulation. [Ref. (6)].

Beam Steering: This involves creating a controlled linear phase gradient across the metasurface so that the reflected electromagnetic wave is redirected toward a desired direction. By appropriately tuning the phase response of individual unit cells, the propagation direction of the wave can be dynamically manipulated, enabling adaptive and directional wavefront control.

Polarization Control: The metasurface modifies the polarization state of the incident wave by introducing anisotropic or asymmetric unit cell designs. This enables conversion between different polarization modes, such as linear to circular or TE to TM, by controlling the phase and amplitude response along orthogonal directions.

Wave Collimation: This is the reverse operation of focusing, where a diverging wavefront is transformed into a planar or highly directive beam. By applying an appropriate phase correction across the surface, the metasurface ensures that waves propagate parallel to each other, reducing divergence.

Splitting: This functionality enables a single incident wave to be divided into multiple reflected or transmitted beams. By superimposing multiple phase

gradients across the metasurface, energy can be distributed into different directions with controlled amplitude, enabling simultaneous multi-directional propagation.

Analog Processing: The metasurface performs mathematical operations directly on the electromagnetic wave, such as differentiation or integration, by tailoring its spatial response.

1.2.2 Applications of RIS –

The following are some of the prominent application domains where RIS technology delivers transformative impact.

5G/6G Heterogeneous Networks: RIS panels mounted on building exteriors, ceilings, or street furniture extend the coverage of macro and small cells by jointly optimizing active precoding at the base station and passive phase shifts at the RIS. This yields significant gains in sum-rate, user fairness, and energy efficiency without deploying additional active base stations - particularly valuable in dense urban mm-wave scenarios where frequent blockage creates intermittent connectivity.

RIS-Assisted SWIPT: Simultaneous Wireless Information and Power Transfer (SWIPT) allows energy-constrained devices - IoT sensors, wearables, and implantable medical equipment - to harvest energy from the same RF

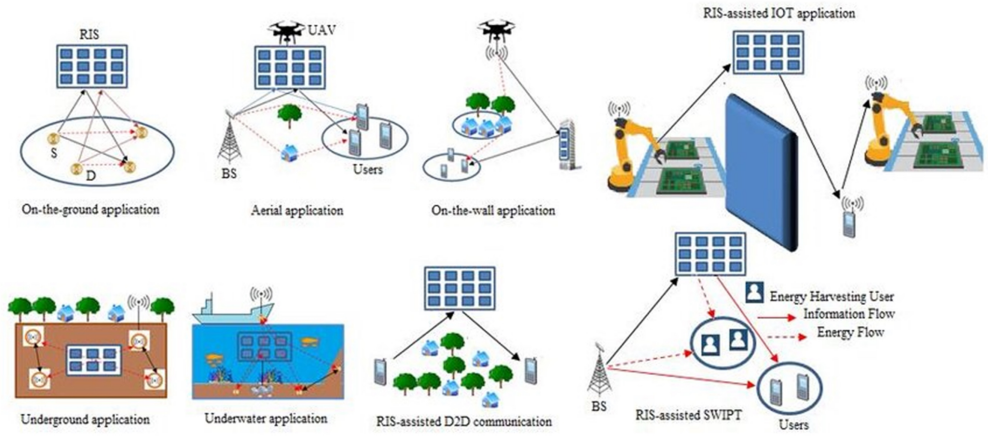

Fig.1.2 Overview of RIS-assisted communication scenarios and SWIPT-enabled IoT applications. [Ref. (6)].

signal carrying information. A low-frequency RIS addresses the core challenge of SWIPT by focusing the RF wavefront onto energy-harvesting receivers through passive beamforming, maximizing incident power density without increasing transmit power. The information is decoded simultaneously via power-splitting or time-switching at the receiver, making this approach well suited for smart agriculture, body area networks, and passive RFID-based IoT systems where battery-free operation is essential.

Integrated Sensing and Communication (ISAC): An RIS can simultaneously steer reflected waveforms toward communication users while focusing a sensing beam on targets of interest. Dynamic phase reconfiguration spatially separates the two functions, reduces their mutual interference, and extends sensing range into regions blocked from the base station - enabling concurrent high-rate data delivery and high-resolution environmental mapping.

RCS Reduction and Stealth Wavefront Engineering: By precisely controlling the phase and amplitude distribution across its surface, an RIS can manipulate the scattered electromagnetic fields to minimize backscattered energy toward the source. This enables radar cross-section (RCS) reduction by redirecting or diffusing the reflected waves into undesired directions. Through engineered phase cancellation and absorption mechanisms, the surface effectively suppresses detectable reflections, allowing it to function as a reconfigurable stealth layer with enhanced control over scattering characteristics.

1.3 Literature Survey on RIS geometry –

In this section, a brief description of the overall thesis structure on RIS-assisted systems is presented. The work is systematically organized from fundamental concepts to advanced multifunctional designs, covering passive, reconfigurable, and switchable RIS architectures along with their practical implementations.

A passive Digitally Coded Metasurfaces (DCMS) operates by arranging subwavelength unit cells with predefined discrete phase responses (coding states) across a surface. When an EM wave is incident, each unit cell imparts a

specific phase shift to the reflected wave based on its geometry. By spatially arranging these phase states, a desired phase gradient is created, enabling controlled wavefront manipulation such as beam steering or focusing. Since it uses no active components or external biasing, the behaviour is fixed once fabricated.

An RIS operates by incorporating active elements such as p-i-n diodes or varactor diodes within each unit cell, enabling dynamic control of its EM response. By adjusting the applied bias, the phase and/or amplitude of the reflected wave from each element can be tuned in real time. This allows the surface to modify its overall phase distribution dynamically, enabling adaptive beam steering, beam shaping, or switching between different functionalities without changing the physical structure.

A switchable RIS geometry operates by toggling between distinct electromagnetic states using active components such as p-i-n diodes. By changing the bias condition, the surface can switch between different functionalities, such as reflection (RIS mode) and absorption. In the OFF state, it behaves as a conventional RIS with controllable phase for beam steering, while in the ON state, introduced losses suppress reflections, enabling absorption. This discrete switching allows multifunctional operation within a single structure.

A brief overview of the passive DCMS, reconfigurable geometry and Switchable RIS, along with the relevant measurement methodologies, has been presented in the subsequent sections.

1.3.1 Phase Distribution Synthesis for Beam Steering –

This section presents the systematic design of a DCMS consisting of an $M \times N$ array of unit cells with dimensions $\Delta x \times \Delta y$, aimed at achieving beam steering under normal incidence as shown in Fig.1.3 (i). The design begins by determining the required phase profile $\Phi(x, y)$ for a desired reflection direction using generalized Snell's law.

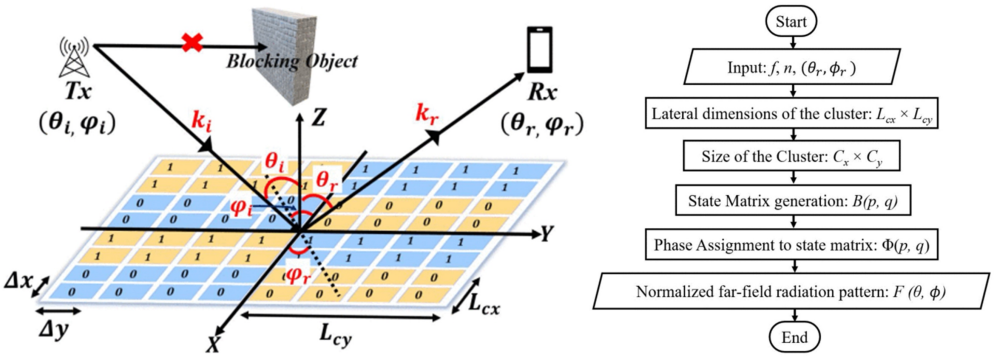

(i) (ii)

Fig.1.3 (i) Illustration of beam steering using coded reflective metasurface. (ii) Systematic design flowchart for digitally coded reflective metasurface design to achieve the desired reflection angle under the illumination of a normal incidence plane wave. [Ref. (8)]

For an incident wave with angles $(\theta_i, \phi_i)$and reflected wave with angles (θ_r, ϕ_r) as shown in Fig. 1.3 (i), the phase gradients along the metasurface are given by:

$$k_i \sin\theta_i \cos\phi_i + \frac{d\Phi}{dx} = k_r \sin\theta_r \cos\phi_r \tag{1.1}$$

$$k_i \sin\theta_i \sin\phi_i + \frac{d\Phi}{dy} = k_r \sin\theta_r \sin\phi_r \tag{1.2}$$

Assuming normal incidence $(\theta_i = 0°, \phi_i = 0°)$ and $k_i = k_r = k_0 = \frac{2\pi}{\lambda_0}$, the equations simplify to:

$$\frac{d\Phi}{dx} = \frac{2\pi}{\lambda_0}\sin\theta_r \cos\phi_r \,, \frac{d\Phi}{dy} = \frac{2\pi}{\lambda_0}\sin\theta_r \sin\phi_r \tag{1.3}$$

The phase difference between adjacent unit cells is defined based on the number of coding bits. For an n-bit metasurface with 2^ndiscrete states:

$$d\Phi = \frac{2\pi}{2^n} \tag{1.4}$$

Using this, the required cluster dimensions along the x- and y-directions are obtained as:

$$L_{cx} = \frac{\lambda_0}{2^n \sin\theta_r \cos\phi_r}, L_{cy} = \frac{\lambda_0}{2^n \sin\theta_r \sin\phi_r} \tag{1.5}$$

These continuous dimensions are mapped to discrete unit cells by:

$$C_x = \left\lfloor \frac{L_{cx}}{\Delta x} \right\rceil, C_y = \left\lfloor \frac{L_{cy}}{\Delta y} \right\rceil \tag{1.6}$$

where $C_x$and C_y represent the number of unit cells in each cluster along x- and y-directions. Next, a **state matrix** $B(p,q)$is generated to assign coding states to each unit cell:

$$B(p,q) = \left(\left\lfloor \frac{p}{C_x} \right\rfloor + \left\lfloor \frac{q}{C_y} \right\rfloor\right) mod 2^n \tag{1.7}$$

where p and q denote the indices of unit cells. The corresponding **phase matrix** is then obtained as:

$$\Phi(p,q) = B(p,q) \times \frac{2\pi}{2^n} \tag{1.8}$$

Finally, the performance of the designed metasurface is evaluated using the array factor formulation to compute the far-field radiation pattern:

$$F(\theta,\phi) = \sum_{p=1}^{M}\sum_{q=1}^{N} exp\left[-j\begin{pmatrix}\Phi(p,q) + k\Delta x(p-0.5)\, sin\,\theta\, cos\,\phi + \\ k\Delta y(q-0.5)\, sin\,\theta\, sin\,\phi\end{pmatrix}\right] \tag{1.9}$$

This systematic procedure as shown in Fig. 1.3(ii), enables precise synthesis of the required phase distribution, allowing accurate beam steering through controlled phase gradients across the DCMS.

1.3.2 Passive DCMS for Single-Beam Steering –

Passive DCMS enable beam steering by spatially arranging unit cells with discrete phase responses, without the need for active components or external biasing. In a single-beam configuration, the metasurface is designed to produce a uniform phase gradient along a specific direction, resulting in the reflection of an incident wave toward a desired angle.

The implementation involves selecting appropriate coding states corresponding to discrete phase values and arranging them periodically to approximate the required linear phase distribution. Each unit cell contributes a fixed phase shift based on its geometry as shown in Fig 1.4 (i), and the

collective response of an array forms a coherent reflected beam as shown in Fig 1.4 (ii). The resolution of beam steering depends on the number of bits used in coding, where higher bit levels provide finer phase quantization and improved steering accuracy.

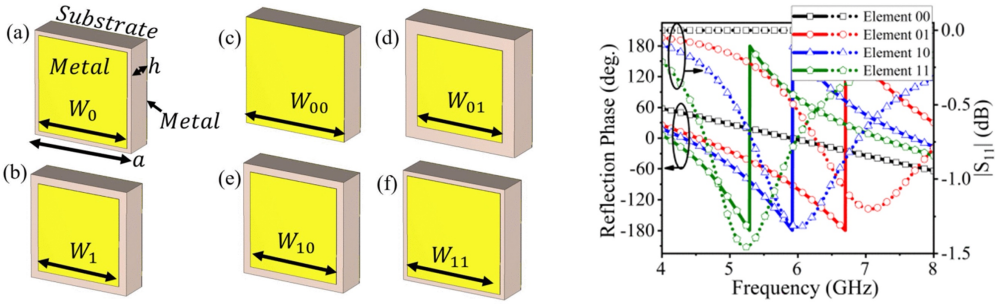

(i) (ii)

Fig.1.4 (i) Unit cell geometry for 1-bit coding (a) element 0 and (b) element 1; for 2-bit coding (c) element 00, (d) element 01, (e) element 10, and (f) element 11 (Dimensions: W0 =8.2 mm, W1 =7.15 mm, W00 =8.45 mm, W01 =6.6 mm, W10 =7.3 mm, W11 =7.75 mm, and a = λ0/6). (ii) Variation of phase and magnitude response with frequency for the unit cell elements of for 2-bit coding. [Ref. (8)]

In this work, the passive DCMS is designed to operate at the desired frequency of 5.9 GHz by optimizing the unit cell geometry to achieve the required phase coverage. The coding sequence is generated based on the calculated phase gradient, ensuring that the reflected wave constructively interferes in the intended direction. The performance of the designed metasurface is evaluated in terms of radiation pattern, beam direction, and sidelobe levels.

Since the structure is passive, its functionality remains fixed after fabrication, making it suitable for applications requiring low complexity and power-efficient beam steering. However, the lack of real-time adaptability motivates further exploration into reconfigurable and multifunctional RIS architectures in subsequent sections.

The steering performance is influenced by the coding resolution and aperture size of the metasurface. Lower-bit designs (1-bit) can achieve the

desired beam direction but may introduce unwanted symmetric beams and higher sidelobe levels due to coarse phase quantization as shown in Fig 1.5 (i). In contrast, higher-bit designs (2-bit) provide improved phase accuracy, resulting in better sidelobe suppression and more precise beam formation as shown in Fig 1.5 (ii). Additionally, the beamwidth is primarily governed by the overall aperture size, with larger surfaces yielding narrower beams.

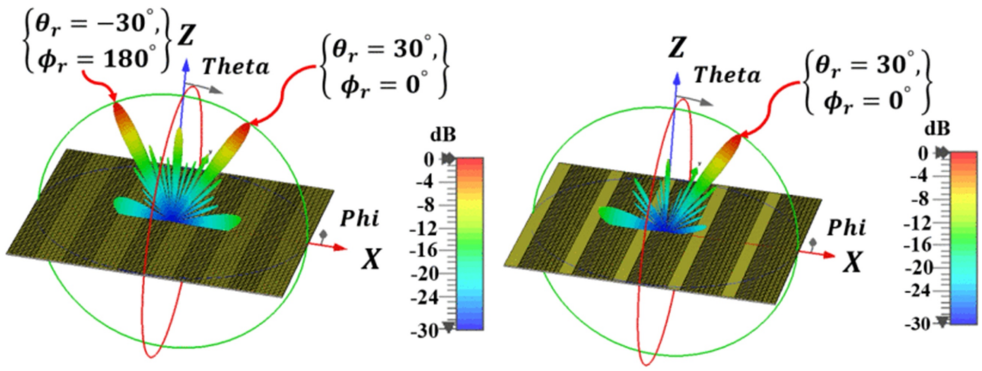

(i) (ii)

Fig.1.5 Normalized radiation pattern of coded metasurface design in CST with a size of $10\lambda_0 \times 10\lambda_0$ showing a reflected beam direction of ($\theta r = 30^\circ, \varphi r = 0^\circ$) for (i) 1-bit coding with SLL–7.6 dB and (ii) 2-bit coding with SLL–12.18 dB. The incident wave is normal to the metasurface. [Ref. (8)]

The designed DCMS is analysed through far-field radiation patterns, where key parameters such as beam direction, half-power beamwidth, and sidelobe levels are evaluated. As a passive structure, the beam direction remains fixed once fabricated, offering a low-complexity and energy-efficient solution for static beam steering applications, while motivating the need for reconfigurable designs in subsequent sections.

1.3.3 Active DCMS or RIS for Beam Steering

In the previous section, a passive DCMS architecture was presented, where the beam steering characteristics remained fixed once the metasurface was fabricated. To introduce dynamic control and reconfigurability, the design is now extended toward an active DCMS architecture, which operates similarly

as an RIS. In this RIS architecture, a column-wise biasing scheme is implemented to control the phase response of the metasurface in a simplified and scalable manner. In contrast to the passive DCMS, the unit cells aligned along a column are electrically connected through shared DC bias lines. These bias lines, realized using narrow metallic strips, distribute a uniform voltage to all the varactors within a column, thereby enforcing identical capacitance and phase response across that column. This approach reduces the complexity of the biasing network and minimizes routing congestion, making it suitable for large-scale implementations. However, it inherently restricts the phase control to one spatial dimension, as phase variations can only be introduced across columns and not along rows.

Ref. [17] presents a unit cell designed as a metal–dielectric–metal multilayer structure fabricated using standard PCB technology. The configuration consists of two metallic patches on the top layer, a continuous metallic ground plane at the bottom, and a dielectric substrate sandwiched in between, as illustrated in Fig. 1.6 (i). A varactor diode is embedded between the top patches, acting as a tunable reactive element whose capacitance varies with the applied reverse bias voltage as shown in Fig.1.6 (ii). This enables dynamic control of the reflection phase of the incident electromagnetic wave.

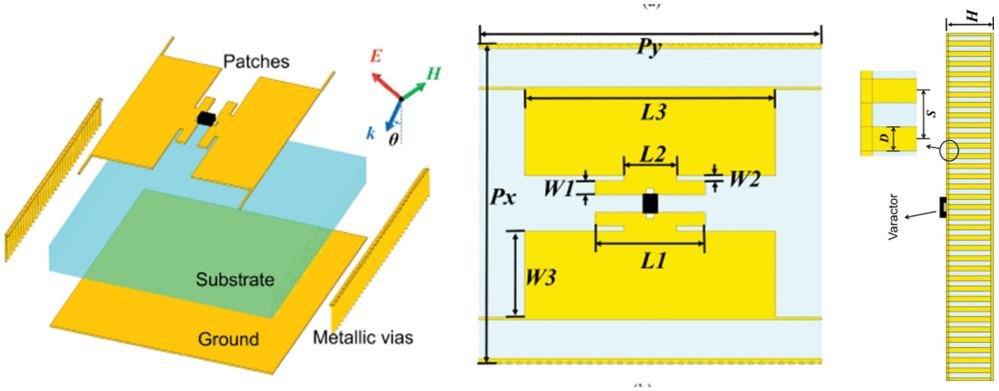

(i) (ii) (iii)

Fig.1.6 Sketch of the proposed meta-atom, in which a varactor is embedded to tune the reflection phase. The metallic vias are employed to reduce the mutual coupling between adjacent meta-atoms and improve the angular insensitivity. (i) Explosive view, (ii) top view and (iii) side view of the meta-atom. [Ref. (17)]

Additionally, metallic vias are introduced between adjacent meta-atoms within the substrate as shown in Fig.1.6 (iii). These vias form a substrate-integrated waveguide (SIW)-like structure that suppresses mutual coupling and mitigates interference caused by multiple internal reflections. As a result, the unit cell exhibits improved angular stability and consistent electromagnetic behaviour under oblique incidence conditions.

The designed RIS achieves 3-bit phase quantization, corresponding to eight discrete phase states with a uniform interval of 45°. By varying the bias voltage applied to the varactor, its capacitance is tuned over a wide range, enabling a total phase shift of approximately 315° as shown in Fig.1.7 (ii). Each bias level corresponds to a specific coding state, allowing digital control of the reflected wavefront. Importantly, the reflection amplitude remains high (greater than −2 dB) across all states as shown in Fig.1.7 (i), indicating efficient energy reflection with minimal loss. The use of a single varactor per unit cell simplifies the design while still achieving precise phase control, which is critical for multibit RIS operation where phase errors must be minimized.

Single beam steering is realized by imposing a linear phase gradient across the metasurface through appropriate column-wise coding of the unit cells. By assigning sequential phase states (e.g., 0° to 315° in 45° steps) across adjacent columns, a spatial phase gradient is created, which redirects the reflected electromagnetic wave according to the generalized Snell's law. This results in anomalous reflection, where the reflected beam deviates from the specular direction. This demonstrates that using a finite array, where a predefined

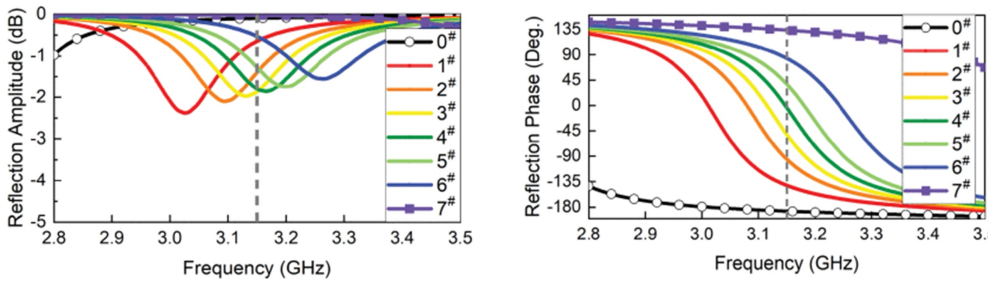

(i) (ii)

Fig.1.7 Numerical simulation results for the (i) amplitudes and (ii) phase responses of the proposed RIS at normal incidence. [Ref. (17)]

coding sequence produces a single dominant reflected beam at a desired angle. However, due to the column-wise biasing scheme, the phase variation is limited to one direction, restricting beam steering to a single plane and limiting the ability to generate more complex beam patterns compared to fully

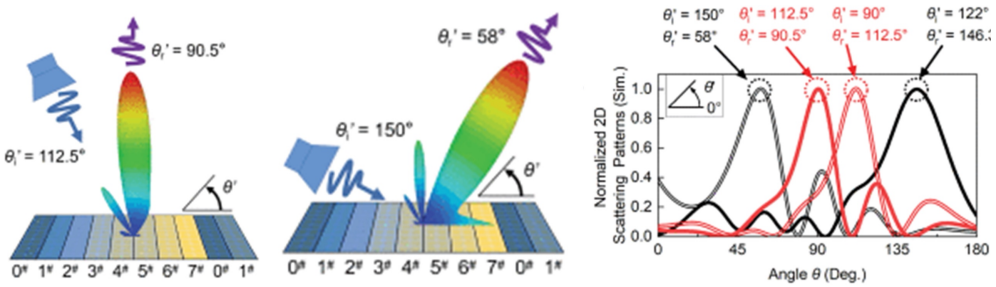

(i) (ii) (iii)

Fig.1.8 Simulated RIS scattering patterns at incident angles θi' of (i) 112.5°, (ii) 150°, (iii) Normalized 2D scattering beam patterns at incident angles of 90°, 122.5°, 150°, and 122°. The RIS angular reciprocity can be obtained from the angle-insensitive meta-atom. [Ref. (17)]

independently controlled unit cells.

In a column-wise biased RIS, all meta-atoms aligned along a column share the same DC bias voltage through common bias lines. As a result, each column produces a uniform reflection phase, and phase variation can only be introduced across columns. This enables the creation of a one-dimensional phase gradient, which is sufficient for basic beam steering applications. The primary advantage of this approach lies in its simplicity: it significantly reduces the number of control lines, biasing circuits, and overall system complexity. This makes it highly scalable and easier to fabricate, especially for large metasurfaces.

However, this simplification comes at the cost of reduced control flexibility. Since all elements in a column are constrained to the same phase state, independent tuning of individual meta-atoms is not possible. Consequently, the RIS can only generate phase gradients in one direction, limiting beam steering to a single plane. Advanced functionalities such as multi-beam generation, beam shaping, or arbitrary wavefront engineering are difficult to achieve with this architecture.

Now moving to the individually biased unit cell design, RIS configuration wherein each element of the surface is independently controlled through a dedicated biasing network. In such an approach, a DC control voltage is applied separately to every unit cell via bias lines or vias, enabling precise tuning of the reactive component embedded within the cell. This independent control mechanism allows each unit cell to exhibit a distinct reflection phase response, thereby enabling the synthesis of arbitrary phase distributions across the entire surface. Unlike column-wise or group-based biasing schemes, individually biased configurations provide maximum degrees of freedom, which is essential for accurate beam shaping and steering, especially in high-resolution multi-bit phase quantization systems.

Ref. [18] presents a unit cell design in which a varactor diode is integrated within a slotted metallic patch to achieve tunable reflection characteristics. The radiating element consists of a metallic patch separated by a narrow slit, across which the varactor diode is embedded, thereby functioning as a voltage-controlled capacitive element. The substrate is realized using a low-loss dielectric material, backed by a ground plane to ensure reflective operation as shown in Fig.1.9 (i). To facilitate independent biasing, dedicated bias vias are introduced to supply DC voltage to the varactor diode, while grounded vias serve as RF grounds as shown in Fig.1.9 (ii) and also contribute inductive effects that enhance phase tunability. Additionally, structural modifications such as asymmetric patch configurations and the inclusion of a surrounding metallic loop improve the effective current path

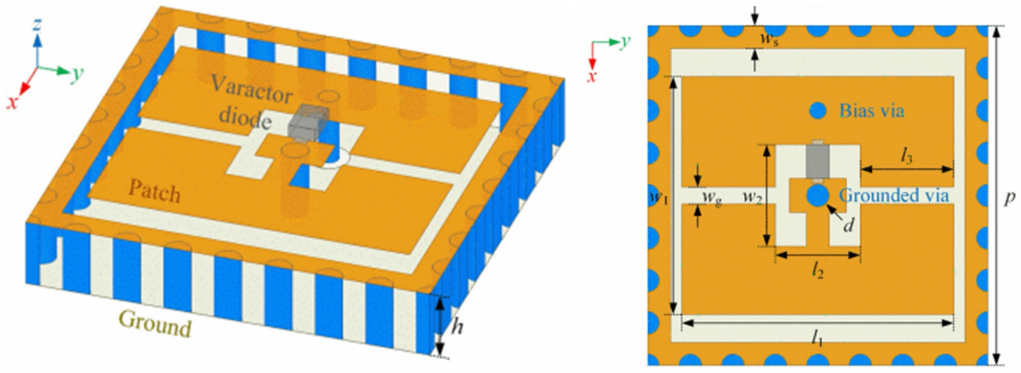

(i) (ii)

Fig.1.9 Geometry of the proposed 3-bit mm-wave RIS unit cell. (i) Front view. (ii) Top view. [Ref. (18)]

and coupling, thereby extending the achievable phase range. The via fence structure further minimizes unwanted surface wave effects and enhances angular stability of the reflection response.

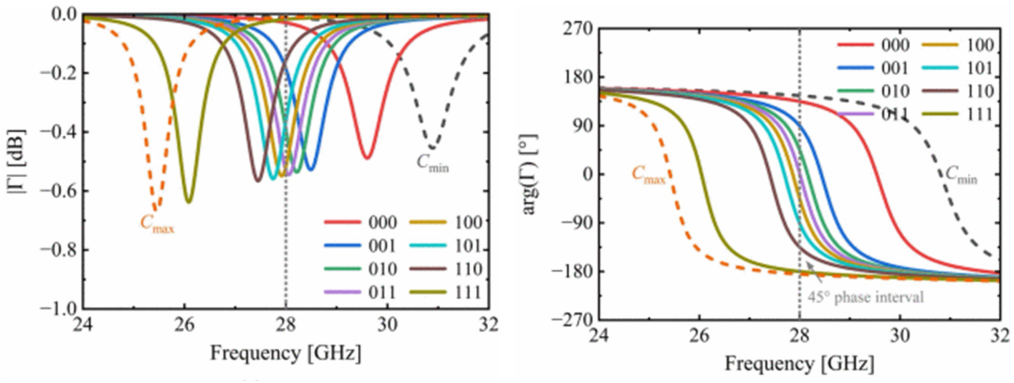

(i) (ii)

Fig.1.10 Reflection coefficients for different operating states. (i) Amplitude. (ii) Phase. Ten curves for different capacitance values are shown, eight of which are identified as the used states (separated by 45° phase interval at 28 GHz), and the other two are the upper and lower limits. [Ref. (18)]

To enable practical beamforming, the unit cell is designed to support multi-bit phase quantization, specifically a 3-bit configuration in this work. This corresponds to eight discrete phase states, each separated by approximately 45°, achieved by varying the reverse bias voltage applied to the varactor diode. The capacitance tuning range of the diode directly controls the reflection phase, resulting in a total phase coverage exceeding 300°, which satisfies the requirement for 3-bit quantization as shown in Fig.1.10 (ii). Importantly, the reflection

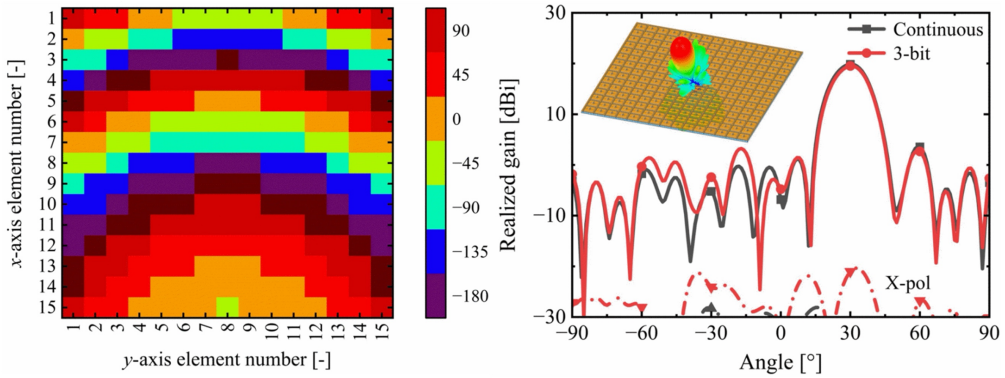

(i) (ii)

Fig.1.11 (i) Quantized phase distribution of the RIS for 30° beam pointing. (ii) Radiation pattern at 28 GHz in φ = 0 plane, inset is the 3D pattern. [Ref. (18)]

magnitude remains relatively constant across all states, with losses maintained below 1 dB, ensuring efficient reflection with minimal amplitude distortion as shown in Fig.1.10 (i). This combination of wide phase coverage and low loss is critical for maintaining high beamforming efficiency.

The beam steering operation is realized by spatially distributing these discrete phase states across the RIS aperture according to a predefined phase gradient. For single-beam steering, a linear phase progression is imposed along one direction of the surface, such that the reflected waves from individual unit cells constructively interfere in a desired direction. By mapping the required phase profile to the nearest available quantized states as shown in Fig.1.11 (i), the RIS effectively redirects the incident electromagnetic wave toward a specific angle. The results presented demonstrates successful beam steering at an off-broadside angle with high directivity and controlled sidelobe levels, validating the effectiveness of the individually biased architecture in practical scenarios as shown in Fig.1.11 (ii).

1.3.4 Switchable RIS Geometry Exhibiting Multifunctional Responses

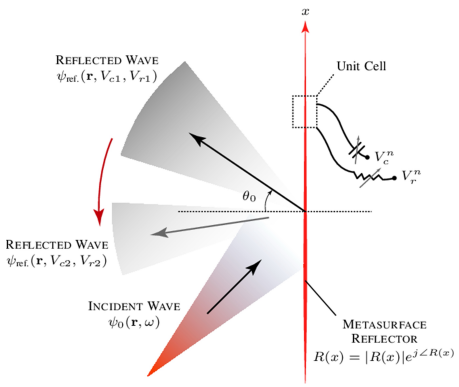

Fig. 1.12. Illustration of a Switchable RIS which transforms incoming incident fields into desired scattered fields via active unit cells consisting of varactor and p-i-n diodes for an independent phase and amplitude control resp. [Ref. (25)]

Building upon the individually controlled RIS architectures discussed in the previous section, Ref. [25] presents a switchable RIS geometry capable of exhibiting multifunctional electromagnetic responses through independent control of the embedded active components. Each unit cell incorporates dedicated biasing lines connected to varactor and p-i-n diodes, enabling dynamic manipulation of

both the reflection phase and magnitude across the metasurface aperture. The varactor diode operates under reverse bias and provides continuous capacitance tuning for phase control, whereas the p-i-n diode functions as a switching element that alters the effective resistance of the resonant structure. Through this combined tuning mechanism, the unit cell can realize different electromagnetic responses such as beam steering, reflection control, and absorption. The overall structure is implemented using a multilayer resonator configuration consisting of metallic patches printed on a grounded dielectric substrate.

In the reported design, the unit cell employs a split-patch resonator geometry in which the varactor diode bridges the central gap and acts as a tunable capacitive element, thereby controlling the resonance and corresponding reflection phase. Simultaneously, the p-i-n diode is incorporated along an additional resonant path to introduce controllable resistive behaviour, enabling modulation of the reflection magnitude, as illustrated in Fig. 1.13(i). The combined effect of these active elements allows the structure to operate as a coupled-resonator system with independently tunable amplitude and phase responses. By appropriately adjusting the bias voltages of the varactor and p-i-n diodes, the unit cell achieves a wide reflection phase variation approaching 315°, along with controllable reflection magnitude ranging from high reflection to partial absorption states, as shown in Fig. 1.13(ii). Such multifunctional tunability significantly enhances the capability

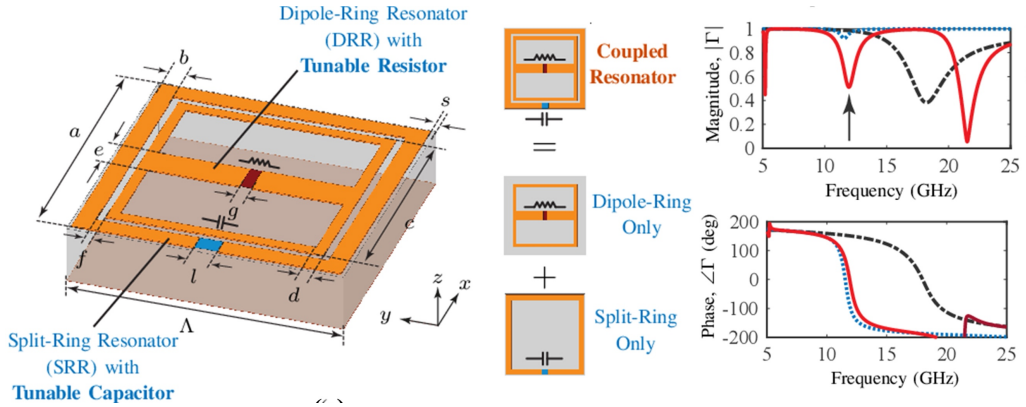

(i) (ii)

Fig.1.13 (i) Proposed metasurface unit cell architecture based on coupled Split Ring Resonator (SRR) and Dipole Ring Resonator (DRR), loaded with tunable capacitor and resistor respectively. (b) FEM-Simulated magnitude and phase of three configuration (R = 25 Ω and C = 0.1 pF). [Ref. (25)].

of the RIS compared to conventional phase-only structures, enabling advanced wavefront engineering operations including beam steering, sidelobe suppression, waveform shaping, and adaptive electromagnetic control, as depicted in Fig. 1.14(ii).

The beam steering functionality of the switchable RIS is achieved by engineering a spatially varying phase distribution across the metasurface aperture. For single-beam steering, a progressive linear phase gradient is introduced along a specific direction of the surface, where each unit cell provides a distinct reflection phase according to its spatial location. As a result, the reflected electromagnetic waves combine constructively in the desired direction, thereby redirecting the main beam away from the specular reflection angle. This controlled wavefront manipulation is governed by the principle of array factor synthesis and generalized Snell's law, enabling programmable steering of the reflected beam.

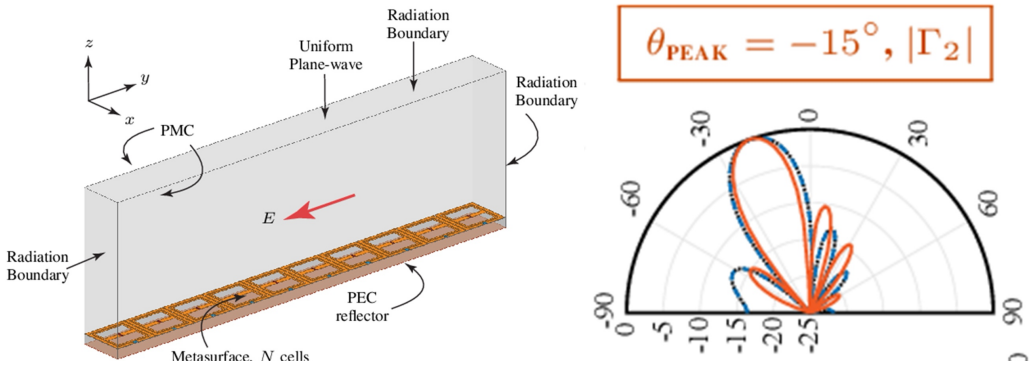

(i) (ii)

Fig.1.14 (i) Illustration of the simulation setup in FEM-HFSS for a finite size metasurface consisting of N unit cells with N lumped resistors and capacitors. The unit cell array is excited with a normally incident linearly polarized plane wave. (ii) Specified peak reflection with beam deflection to -15◦. Normally incident plane-wave and metasurface consists of 20 cells. [Ref. (25)]

In addition to phase manipulation through the varactor diodes, the incorporation of p-i-n diodes enables dynamic control over the reflection magnitude of individual unit cells. This additional degree of freedom allows simultaneous amplitude–phase engineering across the RIS aperture, which significantly improves the overall beamforming performance. By appropriately controlling the reflection magnitude, sidelobe levels can be suppressed and the beam shape can be refined, resulting in enhanced directivity and improved

radiation characteristics compared to conventional phase-only RIS configurations. Such multifunctional control also enables more advanced electromagnetic operations including adaptive beam shaping, scattering control, and waveform engineering.

Although the reported design primarily targets high-frequency and mm-wave operation, the underlying electromagnetic principles remain directly applicable to lower frequency bands such as 3.5 GHz. By appropriately scaling the unit cell dimensions and tuning range of the active components, similar switchable RIS architectures can be implemented for sub-6 GHz wireless communication systems, adaptive beam steering platforms, and multifunctional electromagnetic surfaces.

1.4 Problem Statement –

The existing literature on RIS-assisted systems highlights several limitations in achieving flexible, efficient, and multi-functional beam control using practical metasurface architectures. Higher-order beam generation such as dual and quad beams is not extensively explored at sub-6 GHz frequencies, particularly for communication applications.

For SWIPT applications, passive DCMS designs at lower frequencies face challenges in simultaneously supporting single and multi-beam steering with efficient power distribution. Existing works do not sufficiently address the trade-off between beam steering accuracy and effective energy focusing, which is critical for reliable information and power transfer at 2.5 GHz.

Reconfigurable RIS architectures improve beam control flexibility however, column-wise biasing schemes restrict phase variation to a single dimension, limiting beam steering to one plane. Although individually controlled RIS overcomes this limitation, it introduces increased design and biasing complexity, and its application for simultaneous single and multi-beam steering for sub-6GHz remains insufficiently investigated.

Furthermore, switchable RIS designs reported in literature are primarily focused on high-frequency (mm-wave) operation. Their extension to sub-6 GHz bands, for combined communication and defence applications (including

RCS reduction) is not adequately addressed, particularly in terms of achieving efficient amplitude–phase control with low loss and practical implementation.

Therefore, the problem addressed in this thesis is the design and development of an RIS-assisted system that overcomes these limitations by:

(i) Realizing dual and quad beam steering using passive DCMS at 5 GHz,
(ii) Enabling single and multi-beam steering using passive DCMS at 2.5 GHz for SWIPT applications,
(iii) Designing an individually controlled RIS at 5 GHz for enhanced single and multi-beam steering, and
(iv) Developing a switchable RIS at 3.5 GHz for communication and RCS reduction.

1.5 Organization of the Thesis –

A chapter wise breakup of the present work is as follows:

Chapter 1 presents an overview of Reconfigurable Intelligent Surfaces (RIS), their key functionalities, and applications in wireless communication and RF systems. It reviews existing work on digitally coded metasurfaces (DCMS), individually controlled RIS, and switchable RIS geometries. Finally, the chapter identifies research gaps and formulates the problem statement.

Chapter 2 builds on this foundation by extending the passive DCMS design at 5 GHz, introducing dual and quad-beam steering along with conventional single-beam operation. This enables multi-user support, making the system more aligned with practical wireless scenarios. The approach improves beamforming flexibility and spatial coverage.

Chapter 3 further advances the work by presenting the design and analysis of a passive 3-bit digitally coded metasurface operating at 2.5 GHz. The structure achieves wide phase control through geometrical tuning, enabling

accurate beam steering, sidelobe reduction, and dual-beam operation. Energy focusing is also demonstrated to support SWIPT for IoT systems.

Chapter 4 extends the concept toward dynamic operation by introducing reconfigurability and real-time beam control using p-i-n and varactor diodes. These components enable tuning of phase and amplitude, allowing beam steering to be adjusted through applied bias across the RIS.

Chapter 5 enhances the system by extending the RIS geometry to a switchable metasurface with dual operation. The design acts as an absorber in the ON state and as a conventional RIS in the OFF state with programmable phase control.

Chapter 6 concludes and summarizes the research contributions and outlines potential directions for future work.

Chapter 2: Passive DCMS for Multi-Beam Steering

2.1 Introduction –

Metasurfaces have emerged as a key technology for EM wave manipulation in applications such as wireless communication, radar, and beamforming. Composed of sub-wavelength unit cells, they enable control over reflection, transmission, and wavefront shaping in the microwave regime. While passive metasurfaces offer low complexity and energy-efficient operation, they are limited to fixed functionalities. In contrast, advanced designs focus on improving flexibility through multi-beam generation and enhanced control over radiation characteristics, which are essential for effective beam steering and spatial coverage in next-generation wireless systems.

In this chapter, a passive DCMS design at 5 GHz is introduced, enabling dual and quad-beam steering in addition to conventional single-beam operation. This addresses the limitation of single-beam functionality in existing passive metasurfaces and enables simultaneous multi-directional coverage. Such capability is essential for supporting multi-user communication scenarios, where signals must be directed toward different spatial locations without increasing system complexity. This chapter focuses on the synthesis of appropriate phase distributions and coding strategies required to realize single and multi-beams using a passive structure. Emphasis is placed on improving beamforming flexibility, spatial coverage, and overall radiation performance while maintaining the inherent advantages of low complexity and energy efficiency.

Beam steering is governed by Snell's law as described in section 2.3, which relates incident and reflected wave directions. In metasurfaces, a spatial phase gradient enables anomalous reflection beyond conventional laws. The following section presents the unit cell geometry for the corresponding passive DCMS at 5GHz.

2.2 Unit Cell Geometry –

The performance of the proposed DCMS is primarily determined by the design of the unit cell, which should provide a wide and controllable phase variation with low loss. Figs. 2.1 (i) and 2.1 (ii) illustrate the top and isometric views of the proposed unit cell, respectively. The structure consists of a copper patch printed on an FR4 dielectric substrate ($\varepsilon_r = 4.4$, $\tan\delta = 0.02$), backed by a continuous copper ground plane ($\sigma = 5.8 \times 10^7$ S/m, thickness = 0.035 mm) to ensure complete reflection and eliminate transmission. The unit cell comprises a central square patch of variable length. This geometry enables effective control of surface currents and field distribution, facilitating a wide reflection phase range while maintaining stable amplitude characteristics.

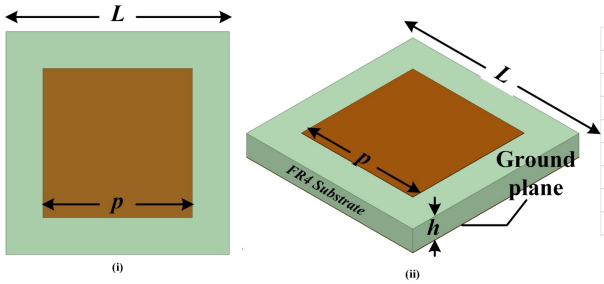

Coding States	p (mm)	Reflection Phase (deg)
#0	12.6	-170
#1	12	-125
#2	11.7	-80
#3	11.5	-35
#4	11.2	10
#5	11.1	55
#6	10.6	100
#7	8.7	145

(iii)

Fig.2.1 Unit cell geometry of the proposed digital coded metasurface: (i) top view, (ii) isometric view. The optimized dimensions are as follows: L = 13 mm, and h = 1.6 mm. (iii) Table 2.1: Eight coding states of the proposed DCMS.

The finite conductivity of metallic patterns and dielectric loss represent the equivalent resistance effect. By varying the geometrical parameters *'p'*, the balance between these effective inductive and capacitive components is altered, resulting in a shift in the resonance characteristics and enabling a wide phase tuning capability. Increasing the substrate thickness enhances the effective inductance and reduces dielectric losses by decreasing field confinement within the lossy substrate, resulting in improved reflection amplitude and smoother phase variation.

Based on this optimization, the substrate thickness is fixed at 1.6 mm, providing an optimal trade-off between low-loss performance and wide phase coverage. The overall unit cell dimension (L) is optimized to 13 mm for operation at 5 GHz. Within this configuration, the reflection amplitude remains below −2.0 dB across the operating frequency band, indicating efficient reflection with minimal loss. A 3-bit coding scheme is achieved, yielding eight discrete phase states (0#–7#) as shown in Table 2.1, realized through appropriate patch length 'p'. These states exhibit uniform phase intervals of approximately 45°, covering the required phase range for effective wavefront control. The corresponding reflection amplitude and phase responses at 5 GHz are presented in Figs. 2.2 (i) and 2.2 (ii), respectively, validating the suitability of the proposed unit cell for digitally coded surface implementation.

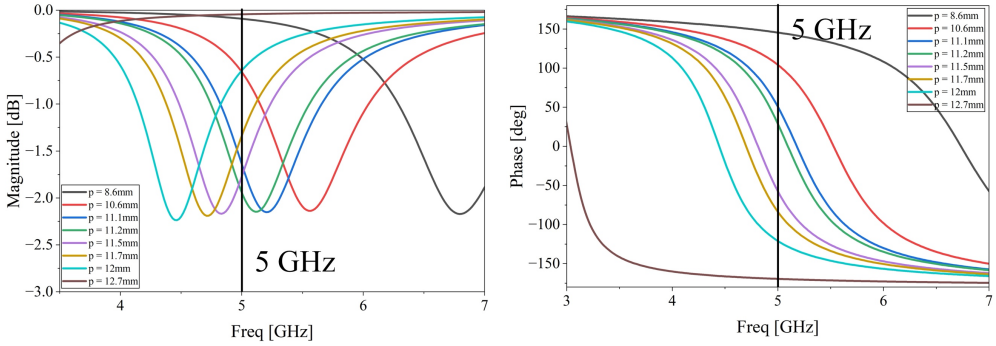

(i) (ii)

Fig.2.2 Simulated S_{11} responses for different patch lengths (p) at 5 GHz: (a) magnitude response, and (b) phase response.

2.3 Generalized Snell's Law –

In the far-field region, the EM wave behaves as a plane wave, with each point on the wavefront sharing the same phase. The shape of the EM wave can be modified if the phase at different points on the wavefront is adjusted. When an EM wave impinges on a metasurface, the presence of subwavelength resonators on the surface can contribute to phase gradients and cause anomalous reflection at other angles. The equation, derived from generalized Snell's law, is presented below:

$$\sin\theta_r - \sin\theta_i = \frac{\lambda_0}{2\pi n_i}\frac{d\Phi}{dx} \qquad (2.1)$$

where, λ_0 represents the wavelength of the incident EM wave, and n_i is the refractive index of the medium where the DCMS is placed. The angles θ_r and θ_i correspond to the reflection and incident angles, respectively. The phase difference between two incidence points is $d\Phi$, and the corresponding separation distance is dx. As observed from Equation (2.1), the reflection angle can be controlled by varying the phase difference ($d\Phi$) between the neighbouring incidence points.

Each unit cell in a metasurface can produce a distinct reflection phase by adjusting its geometric dimensions or material properties. By arranging these unit cells appropriately, the desired phase gradient can be attained at specific locations, enabling the manipulation of the overall wavefront to produce anomalous reflection. Although a continuous progressive phase shift between successive unit cells is theoretically possible, fabrication constraints often make it challenging to achieve precise phase resolution. This limitation leads to the selection of a few discrete reflection phases rather than all possible values, effectively discretizing the phase profile. When the maximum phase shift has a span of 2π, an equal phase interval of $2\pi/(2^n - 1)$ can be defined for an n-bit system, resulting in 2^n distinct phase states. For example, in a 3-bit system, there are eight discrete phase states, each separated by a 45° interval, covering a total phase range of (or above) 315°.

The proposed unit cell, as illustrated in Fig. 2.1, exhibits an overall phase shift range of 315° (from −170° to +145°) as can be seen in Fig. 2.2(ii). To design a 3-bit PGMS structure using this unit cell, eight coding states are considered, each corresponding to different patch lengths with a 45° phase interval. To verify anomalous reflection, unit cells are arranged with a progressive phase shift to achieve the desired phase gradient. Based on this phase synthesis approach, the following sections present the implementation of *n*-bit RIS geometries for single-beam (normal and oblique incidence) and multi-beam steering.

2.4 Single-Beam Steering Operation –

Once the principle of anomalous reflection is established, DCMS structures are designed to demonstrate beam steering in different directions. The metasurface is analysed under both normal and oblique incidence from the far field, and DCMS designs with 1-bit and 3-bit coding states are implemented. It is noteworthy that a total of 30×30 unit cells have been considered for all the cases, having an overall dimension of $6.5\lambda_0 \times 6.5\lambda_0$ (where λ_0 is the wavelength at the operating frequency 5 GHz). It is the relative placement of the unit cells based on the required phase profile, which results in the beam steering in different directions. After designing the DCMS structures, full-wave simulations have been performed using the finite element boundary integral (FEBI) set up in Ansys HFSS software.

2.4.1 Normal Incidence –

For normal incidence, the metasurface is designed to steer the reflected beam toward a desired angle by introducing a spatial phase gradient. In the 1-bit coding configuration, the surface provides two (2^1) discrete phase states with an intended phase difference of 180°. The selected phase values, −170° and +10°, are extracted from the 3-bit configuration, as summarized in Table 2.1. These unit cells are spatially arranged to realize the required phase gradient corresponding to a target reflection angle of $\theta_r = 30°$. The resulting phase distribution and normalized radar cross-section (RCS) pattern confirm that the reflected beam is steered toward the desired direction, as presented in Fig. 2.3.

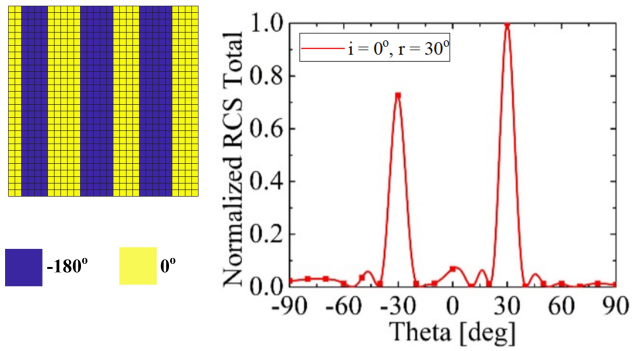

Fig.2.3 Simulated response of the proposed 1-bit RIS geometry for single beam steering under normal incidence conditions.

To improve beam quality and reduce sidelobes, a 3-bit coding scheme is employed, providing eight (2^3) discrete phase states with a finer resolution of 45°. The corresponding phase values are used to achieve a more accurate phase profile for the same steering angle of $\theta_r = -45°$ as shown in Fig 2.4. The results show a sharper main beam with reduced sidelobe levels compared to the 1-bit case, owing to the smoother phase transition across the metasurface.

This demonstrates that higher phase quantization significantly enhances beamforming performance under normal incidence. However, in practical scenarios, EM waves often arrive at oblique angles, which can affect the phase response and steering accuracy. Therefore, the following section investigates the beam steering performance under oblique incidence using the 3-bit configuration.

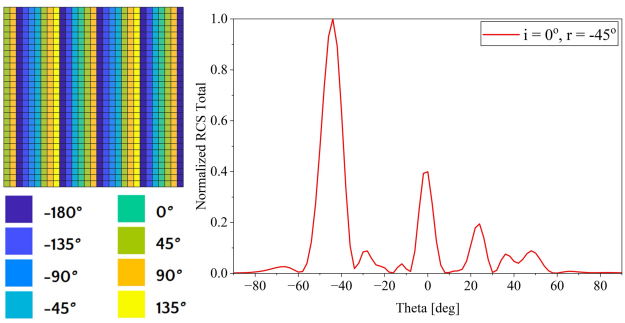

Fig.2.4 Simulated response of the proposed 3-bit RIS geometry for single beam steering under normal incidence conditions.

2.4.2 Oblique Incidence –

To further evaluate the robustness of the proposed design, oblique incidence scenarios are considered. In this case, the incident wave is applied at $\theta_i = 20°$, and the metasurface is designed to steer the reflected beam toward $\theta_r = 15°$, as shown in Fig. 2.5. The 3-bit coded structure maintains the required phase gradient even under tilted illumination, resulting in effective beam steering. The simulated results show that the main beam direction closely follows the theoretical prediction, demonstrating good angular stability.

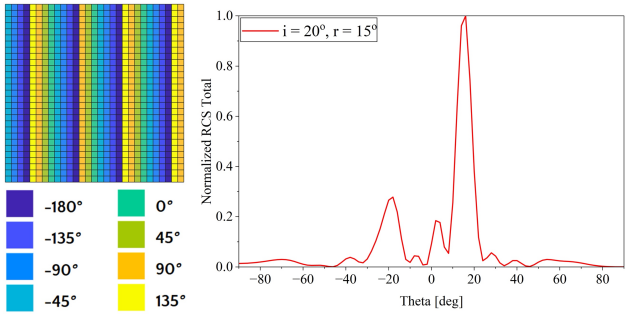

Fig.2.5 Simulated response of the proposed 3-bit RIS geometry for single beam steering under oblique incidence conditions.

In another oblique incidence case, the incident angle is $\theta_i = 15°$, and the reflected beam is steered toward $\theta_r = 30°$. Similar to the previous case, the metasurface successfully redirects the incident wave to the desired angle, confirming the consistency of phase control under varying incidence conditions as shown in Fig. 2.6. The use of a 3-bit configuration ensures finer phase resolution, which helps preserve beam accuracy and reduces distortion in the reflected pattern.

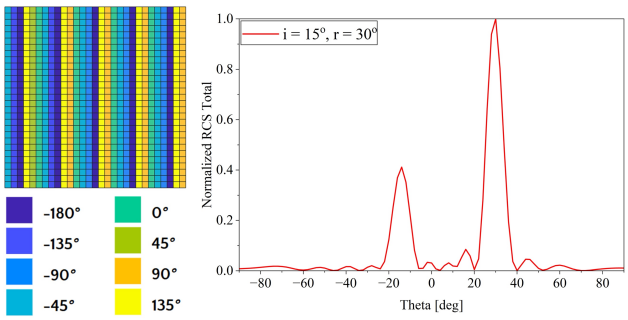

Fig.2.6 Simulated response of the proposed 3-bit RIS geometry for single beam steering under oblique incidence conditions.

These results confirm that the proposed metasurface design performs reliably under both normal and oblique incidence conditions, maintaining stable beam steering characteristics. Having validated single-beam steering performance, the next section focuses on extending the design to achieve multi-beam steering using appropriate coding strategies.

2.5 Multi-Beam Steering Operation –

After establishing single-beam steering, the concept is extended to multi-beam operation by appropriately engineering the phase distribution across the metasurface. Unlike single-beam steering, where a linear phase gradient is imposed, multi-beam generation requires superposition of phase profiles to simultaneously direct energy toward multiple directions. The metasurface is analysed under far-field excitation, and both dual and quad-beam configurations are realized using suitable coding strategies based on 3-bit phase states. The following subsections present the design and analysis of dual-beam and quad-beam steering configurations, highlighting their phase synthesis approach and radiation performance.

2.5.1 Dual-Beam Steering –

In dual-beam steering, two desired reflection angles, θ_{r1} and θ_{r2}, are considered. Based on generalized Snell's law, the corresponding phase profiles are given by:

$$\Phi_1(x) = \left(\frac{2\pi}{\lambda}\right) x(\sin\theta_{r1} - \sin\theta_i) \tag{2.2}$$

$$\Phi_2(x) = \left(\frac{2\pi}{\lambda}\right) x(\sin\theta_{r2} - \sin\theta_i) \tag{2.3}$$

To generate both beams simultaneously, the overall phase distribution is obtained using the superposition principle:

$$\Phi(x) = \arg\left(e^{j\Phi_1(x)} + e^{j\Phi_2(x)}\right) \tag{2.4}$$

This combined phase profile enables the metasurface to split the reflected energy into two distinct directions corresponding to $\theta_{r1}$and θ_{r2}. In the proposed passive DCMS, this is achieved by properly arranging discrete coding states of the unit cells, resulting in efficient dual-beam steering with low design complexity.

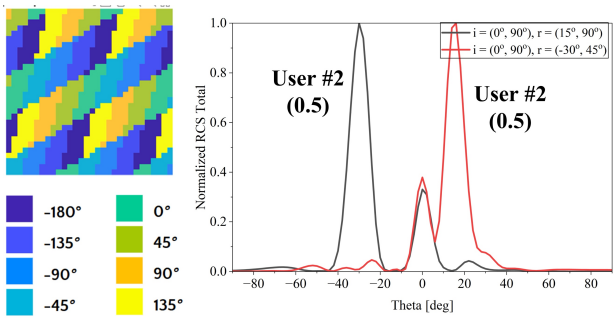

Fig.2.7 Simulated response of the proposed 3-bit RIS geometry for dual beam steering under normal incidence conditions and with equal power distribution

Based on the synthesized phase distribution, the proposed metasurface is extended to achieve dual-beam operation using a 3-bit coding scheme. In this configuration, the discrete phase states are arranged to approximate the combined phase profile, enabling simultaneous reflection toward two distinct angles. The corresponding radiation patterns and phase distributions, as shown in Fig. 2.7, confirm that the metasurface effectively splits the incident energy into two directed beams with good angular accuracy.

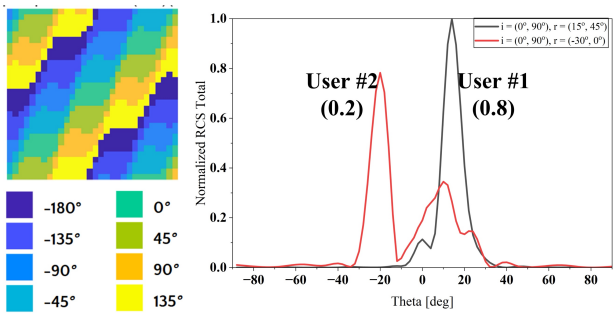

Fig.2.8 Simulated response of the proposed 3-bit RIS geometry for dual beam steering under normal incidence conditions and with unequal power distribution

Furthermore, controlled power distribution between the beams is demonstrated by modifying the phase synthesis. A dual-beam case with a power ratio of 4:1 is realized, as shown in Fig. 2.8, highlighting the capability of the proposed design to not only generate multiple beams but also regulate their relative strengths. Having demonstrated dual-beam functionality, the following section extends the concept to quad-beam steering for further enhancement of spatial coverage.

2.5.2 Quad-Beam Steering –

In quad-beam steering, four desired reflection angles θ_{r1}, θ_{r2}, θ_{r3}, and θ_{r4} are considered simultaneously. Based on generalized Snell's law, the individual phase distributions corresponding to each reflection direction are expressed as:

$$\Phi_k(x) = \left(\frac{2\pi}{\lambda}\right).x.(\sin\theta_{rk} - \sin\theta_i) \tag{2.5}$$

where k = 1,2,3,4. To simultaneously generate all four reflected beams, the overall phase distribution is synthesized using the superposition principle, given by:

$$\Phi(x) = \arg\left(e^{j\Phi_1(x)} + e^{j\Phi_2(x)} + e^{j\Phi_3(x)} + e^{j\Phi_4(x)}\right) \tag{2.6}$$

This combined phase distribution enables the metasurface to divide the reflected energy into four distinct directions corresponding to θ_{r1}, θ_{r2}, θ_{r3}, and θ_{r4}. Based on the synthesized phase profile, a 3-bit DCMS is designed to realize quad-beam steering with equal power distribution among all four beams. The steering directions are selected as follows: User#1 – $\theta_{r1} = 30°$, $\phi_{r1} = 0°$, User#2 – $\theta_{r2} = -30°$, $\phi_{r2} = 0°$, User#3 – $\theta_{r3} = 45°$, $\phi_{r3} = 45°$, and User#4 – $\theta_{r4} = 45°$, $\phi_{r4} = 90°$.

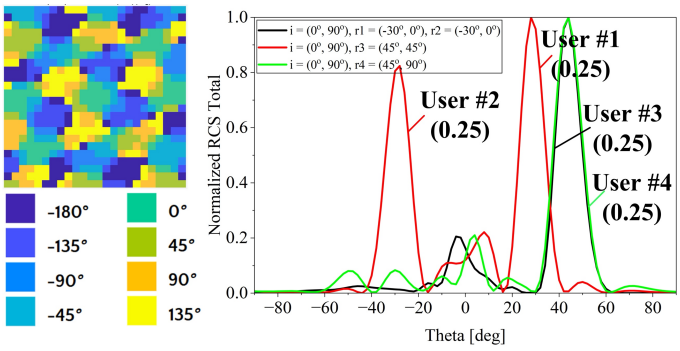

Fig.2.9 Simulated response of the proposed 3-bit RIS geometry for quad beam steering under normal incidence conditions and with equal power distribution

The discrete coding states are spatially arranged to approximate the synthesized phase distribution, thereby enabling uniform splitting of the incident energy into the four desired directions. The simulated radiation patterns confirm the formation of four well-defined beams with nearly equal

amplitudes, validating the effectiveness of the proposed coding strategy for multi-user beam steering. Furthermore, the finer phase resolution offered by the 3-bit configuration improves the accuracy of the phase synthesis, resulting in enhanced beam symmetry, lower distortion, and reduced undesired scattering components.

The results confirm that the proposed metasurface can achieve efficient quad-beam steering with balanced power distribution and stable radiation characteristics as shown in Fig. 2.9. This highlights its potential for applications requiring simultaneous multi-user coverage and enhanced spatial diversity. With the successful realization of single, dual, and quad-beam steering, the overall capability of the passive DCMS is established. The following section concludes the chapter by summarizing the key findings and outcomes.

2.6 Conclusion –

This chapter presented the design and analysis of a passive DCMS operating at 5 GHz for beam steering applications. The fundamental principle of anomalous reflection based on generalized Snell's law was discussed, followed by the synthesis of required phase distributions using discrete coding states. A 3-bit unit cell configuration was employed to achieve a wide phase coverage, enabling accurate realization of desired phase gradients. The performance of the metasurface was first validated for single-beam steering under both normal and oblique incidence conditions, demonstrating good agreement between theoretical predictions and simulated results.

The concept was then extended to multi-beam steering, where dual- and quad-beam configurations were realized using appropriate phase synthesis techniques. The metasurface successfully generated multiple beams with controlled directions, and in the quad-beam case, equal power distribution among all beams was achieved. The results highlight the effectiveness of higher phase quantization in improving beam quality, reducing sidelobes, and enhancing overall radiation performance.

Overall, the proposed passive DCMS provides a low-complexity and energy-efficient solution for single and multi-beam steering at 5 GHz. While the design offers fixed functionality after fabrication, it demonstrates significant capability in achieving multi-directional coverage, making it suitable for applications requiring static beamforming. This also establishes a foundation for more advanced reconfigurable and switchable RIS architectures discussed in subsequent chapters.

Chapter 3: Passive DCMS for Beam Steering and SWIPT

3.1 Introduction –

In the previous chapter, we have demonstrated the capability of passive DCMS at 5 GHz for single and multi-beam steering using appropriate phase synthesis techniques. The design established that by arranging discrete coding states across a metasurface, controlled wavefront manipulation can be achieved, enabling efficient beam steering with low complexity.

Building on this foundation, this chapter now focuses on the design of passive DCMS operating at a lower frequency of 2.5 GHz, where larger wavelengths allow the realization of electrically larger apertures with improved wave interaction. Digitally coded metasurfaces, composed of sub-wavelength unit cells with discrete phase states, enable precise control over reflected electromagnetic waves through spatial phase engineering. By introducing appropriate phase gradients across the surface, the incident wave can be redirected or focused toward desired locations, providing enhanced control over spatial energy distribution.

In addition to beam steering, this chapter explores the potential of DCMS for simultaneous wireless information and power transfer (SWIPT). By concentrating electromagnetic energy at specific regions, the metasurface can improve power delivery while maintaining communication functionality. This approach enables efficient utilization of reflected energy and provides a framework for integrating beamforming and energy focusing within a single passive structure. The chapter further investigates different coding configurations to achieve improved beam characteristics, forming the basis for SWIPT-enabled metasurface designs.

3.2 Unit Cell Geometry –

The performance of the proposed DCMS is governed by the design of the unit cell, which must provide a wide and controllable phase variation with

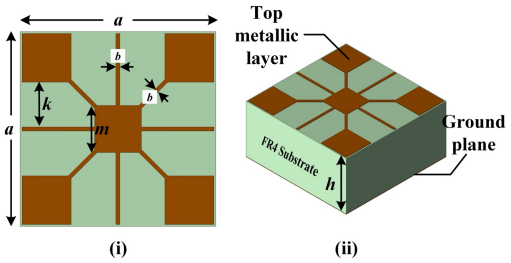

Coding States	k (mm)	m (mm)	Reflection Phase (deg)
#0	1	3.9	-174
#1	1	1.5	-129
#2	6.2	0.5	-84
#3	4.6	1.3	-39
#4	8.2	2.3	6
#5	1	3.7	51
#6	5.8	3.1	96
#7	4.2	4.5	141

(iii)

Fig.3.1 Unit cell geometry of the proposed digital coded metasurface: (i) top view, (ii) isometric view. The optimized dimensions are as follows: L = 10 mm, and h = 4.8 mm. (iii) Table 3.1: Eight coding states of the proposed DCMS.

minimal loss. The unit cell consists of a copper patch printed on an FR4 substrate ($\varepsilon_r = 4.4$, $\tan\,\delta = 0.02$), backed by a continuous ground plane to ensure complete reflection. The geometry follows a symmetric configuration with a central patch connected to orthogonal arms extending toward corner patches, enabling effective control of surface currents and field distribution as shown in Fig. 3.1. This structure facilitates a wide reflection phase range while maintaining stable amplitude characteristics.

The EM behaviour of the unit cell can be interpreted using an equivalent RLC model, where metallic paths introduce inductance and gaps contribute to capacitance, while material losses account for resistance. By varying key geometrical parameters, the resonance characteristics can be tuned to achieve the desired phase response. Additionally, the substrate thickness plays a crucial role in determining performance; increasing thickness improves phase variation and reduces loss. An optimized thickness of 4.8 mm is selected to balance phase coverage and reflection efficiency, with an overall unit cell dimension of 10 mm for operation at 2.5 GHz.

Using this optimized configuration, a 3-bit coding scheme is realized, providing eight discrete phase states with approximately 45° intervals. The reflection amplitude remains better than −1.6 dB across the operating frequency, indicating low-loss performance as shown in Fig. 3.2 (i). These phase states enable accurate wavefront shaping, making the unit cell suitable for implementing DCMS as shown in Fig. 3.2 (ii). Based on this unit cell design, the next section presents beam steering operations.

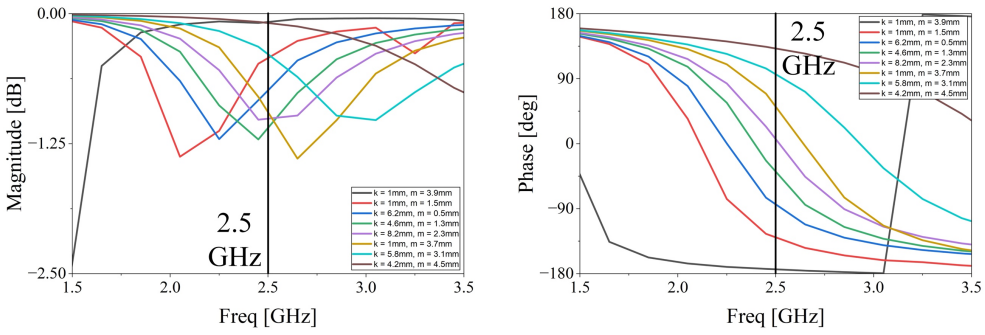

(i) (ii)

Fig.3.2 Simulated S_{11} responses for different patch lengths (k) and (m) at 2.5 GHz: (i) magnitude response, and (ii) phase response.

3.3 Beam Steering Operation –

As described by Snell's law in Equation 2.1, beam steering is achieved by introducing a spatial phase gradient across the metasurface. When a plane wave from the far-field region impinges on the digitally coded metasurface, the required wavefront manipulation is realized by arranging unit cells with distinct reflection phases in a progressive manner. This controlled phase variation enables anomalous reflection, directing the reflected wave toward a desired angle.

The proposed structure consists of a 72×72 array of unit cells, corresponding to an aperture size of approximately $6\lambda_o$ x $6\lambda_o$ at the operating frequency of 2.5 GHz. Being a passive configuration, the required phase distribution is achieved purely through geometrical design, without the need for external biasing or control circuits. Each unit cell is assigned a specific

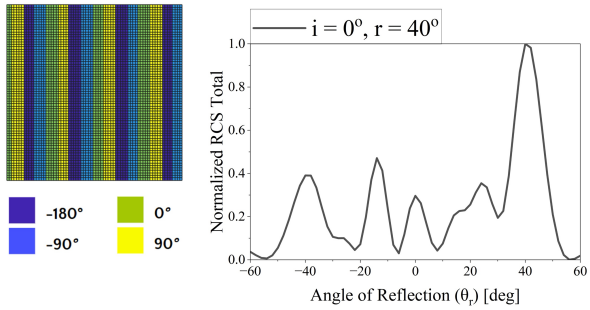

Fig.3.3 Simulated response of the proposed 2-bit RIS geometry for single beam steering under normal incidence conditions.

phase state based on the coding scheme, and their spatial arrangement establishes the necessary phase gradient across the surface to enable beam steering.

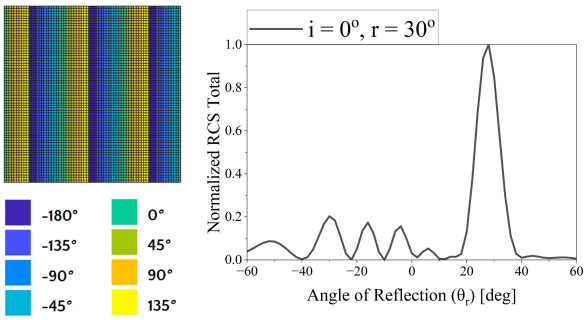

Fig.3.4 Simulated response of the proposed 3-bit RIS geometry for single beam steering under normal incidence conditions.

3.3.1 Single-Beam Steering –

For single-beam steering under normal incidence, the metasurface is designed to generate a desired phase gradient to redirect the reflected wave toward a specified angle. In the 2-bit coding configuration, the surface provides four (2^2) discrete phase states with an intended phase difference of 90°. The selected phase values, −174°, −84°, +6°, and +96°, are extracted from the 3-bit design and arranged to realize the required phase gradient corresponding to a target reflection angle of $\theta_r = 40°$. The resulting phase distribution and normalized radar cross-section (RCS) pattern confirm successful beam steering toward the desired direction as shown in Fig. 3.3.

To enhance beam quality and reduce sidelobe levels, a 3-bit coding scheme is employed, providing eight (2^3) discrete phase states with a finer resolution

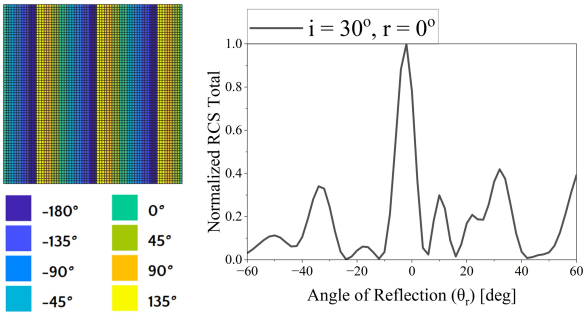

Fig.3.5 Simulated response of the proposed 3-bit RIS geometry for single beam steering under oblique incidence conditions.

of 45°. These phase states enable a more accurate approximation of the required phase profile. For single-beam steering, the unit cells are arranged to achieve a reflection angle of $\theta_r = 30°$. The simulated results show a sharper main beam with reduced sidelobes as shown in Fig. 3.4, compared to the 2-bit configuration, owing to smoother phase transitions across the metasurface.

To evaluate performance under practical conditions, oblique incidence is also considered. In this case, the incident wave is applied at $\theta_i = 30°$, and the reflected beam is steered toward $\theta_r = 0°$ as shown in Fig. 3.5. The metasurface maintains the desired phase gradient under tilted illumination, demonstrating good angular stability. The results show close agreement with theoretical predictions, validating the effectiveness of the proposed design for both normal and oblique incidence conditions.

3.3.2 Dual-Beam Steering –

The proposed metasurface is further extended to achieve dual-beam steering using a 3-bit coding scheme. In this approach, two desired reflection angles θ_{r1} and θ_{r2} are considered, and the corresponding phase profiles $\Phi_1(x)$ and $\Phi_2(x)$ are obtained based on generalized Snell's law, as given in equation (2.2) and (2.3). To simultaneously generate both beams, the overall phase distribution $\Phi(x)$ is synthesized using the superposition of these individual phase responses, as expressed in equation (2.4). This combined phase profile enables controlled splitting of the reflected wave into two distinct directions.

In practical implementation, the continuous phase distribution is approximated using discrete coding states of the 3-bit DCMS. The unit cells

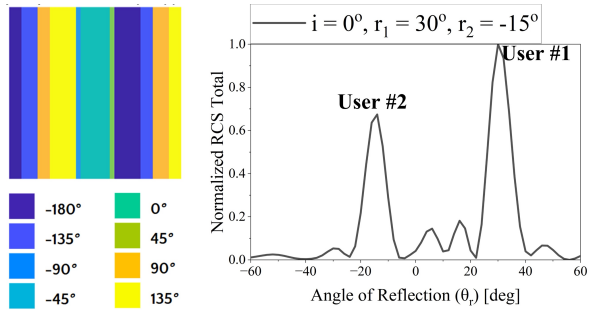

Fig. 3.6 Simulated response of the proposed 3-bit RIS geometry for dual beam steering under normal incidence conditions and with equal power distribution.

are arranged such that the required phase combination derived from equation (2.4) is realized across the metasurface aperture. This spatial arrangement ensures that the reflected waves constructively interfere along the desired directions, resulting in the formation of two beams. The radiation patterns and corresponding phase distributions, as shown in Fig. 3.6, validate that the metasurface effectively achieves dual-beam steering with good angular accuracy.

Furthermore, controlled power distribution between the beams is demonstrated by modifying the phase synthesis derived from equations (2.2)–(2.4). A dual-beam case with a power ratio of 4:1 is realized, as illustrated in Fig. 3.7, highlighting the capability of the design to regulate the relative beam strengths. These results demonstrate that, through appropriate coding and phase engineering, the proposed metasurface can efficiently realize dual-beam operation while maintaining low complexity, forming a basis for further extension to multi-beam configurations.

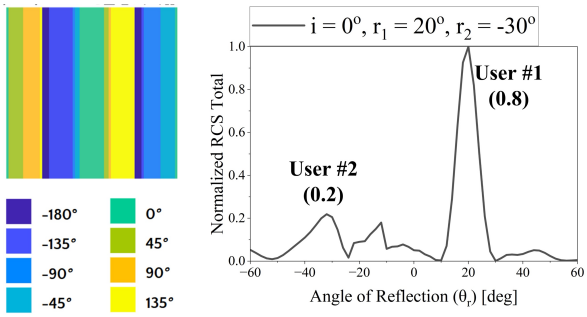

Fig. 3.7 Simulated response of the proposed 3-bit RIS geometry for dual beam steering under normal incidence conditions and with unequal power distribution

3.4 SWIPT Enabled IoT Application –

SWIPT has emerged as a promising technique to support energy-constrained IoT devices in remote environments. In a SWIPT framework, a single EM wave simultaneously carries both information signals and harvestable RF energy, enabling IoT nodes to operate without dedicated power sources. However, in practical deployments, physical obstructions frequently block the direct line-of-sight (LOS) path between the base station and IoT

receiver nodes, causing severe degradation in received signal quality and harvested power levels.

To overcome this limitation, an RIS is deployed to assist SWIPT operation under non-line-of-sight (NLOS) conditions, as illustrated in Fig. 3.8. As shown, the base station, the passive DCMS panel, and all the IoT sensor nodes are positioned on the same side of the reflecting surface, with a physical obstacle completely eliminating the direct communication link. The DCMS comprises an array of metallic patches whose phase responses are digitally configured. By imposing a designed phase distribution across the patch aperture, the DCMS manipulates the incident EM wavefront from the base station.

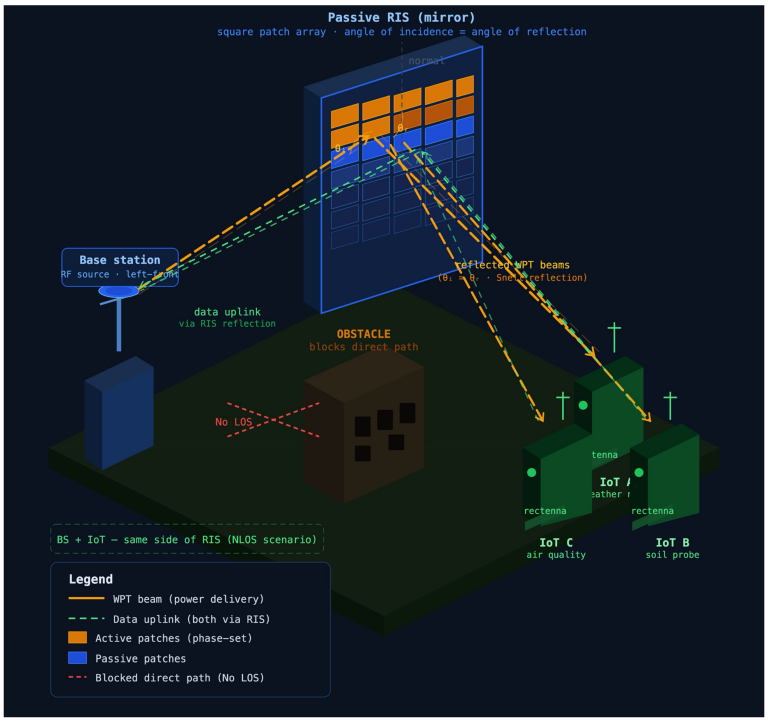

Fig. 3.8 Illustration of the proposed RIS-assisted SWIPT system for IoT in NLOS conditions using Snell's law-based beam steering.

Governed by Snell's law of reflection - where the angle of incidence equals the angle of reflection about the surface normal - the DCMS steers the incoming signal toward each IoT device through precisely directed reflected beams (anomalous reflection). This simultaneously delivers both information and RF energy, restoring the SWIPT link purely through passive reflection. As seen in

Fig. 3.8, the distinct beams are formed, each directed toward a separate IoT node, where onboard rectenna circuits convert the received EM energy into DC power for device operation. The reflected link is also bidirectional - sensor data from each IoT node is routed back to the base station via the same RIS reflection path, maintaining uplink communication alongside downlink power transfer.

The DCMS enhances spatial coverage in NLOS regions while concentrating electromagnetic energy toward specific targets through passive beamforming, improving harvesting efficiency without active amplification. The DCMS further enables this through discrete phase coding and passive beam steering, offering low hardware complexity suitable for scalable SWIPT-enabled IoT deployments. Without RIS assistance, the blocked LOS path would result in severe attenuation, rendering both communication and energy harvesting insufficient for reliable IoT operation.

3.5 Conclusion –

This chapter presented the design and analysis of a passive DCMS operating at 2.5 GHz for beam steering and SWIPT-enabled IoT applications. The unit cell was optimized to achieve wide phase coverage with low reflection loss, enabling effective implementation of multi-bit coding schemes. Using this configuration, single-beam steering was demonstrated under both normal and oblique incidence conditions, validating the capability of the proposed structure to achieve accurate phase-controlled wavefront manipulation.

The concept was further extended to multi-beam steering, where dual-beam configurations were realized using appropriate phase synthesis based on generalized Snell's law. The metasurface successfully generated multiple beams with controlled directions and power distribution, demonstrating flexibility in spatial energy allocation. The use of a 3-bit coding scheme provided improved phase resolution, resulting in better beam quality, reduced

sidelobe levels, and enhanced overall performance compared to lower-bit implementations.

In addition, the application of the proposed DCMS in SWIPT-enabled IoT scenarios was investigated under NLOS conditions. The results showed that the RIS-assisted system can effectively restore communication links and enhance energy delivery by redirecting and focusing electromagnetic waves. Overall, the passive DCMS provides a low-complexity and energy-efficient solution for combined communication and power transfer. However, the lack of real-time adaptability in passive designs motivates the need for more advanced architectures, which is addressed in the next chapter through the design of individually controlled RIS for dynamic beam steering and enhanced functionality.

Chapter 4: Dynamically - Controlled RIS Geometry

4.1 Introduction –

In the previous chapter, a passive DCMS operating at 2.5 GHz has been presented for beam steering and SWIPT-enabled applications. The design has demonstrated effective wavefront manipulation through fixed coding arrangements, enabling controlled reflection and spatial energy distribution. However, a key limitation of passive DCMS structures is that the phase profile is predefined during the design stage and remains unchanged after fabrication. As a result, the reflection direction is fixed, restricting the metasurface to serve only a specific spatial direction or a limited set of users as shown in Fig. 4.1 (i).

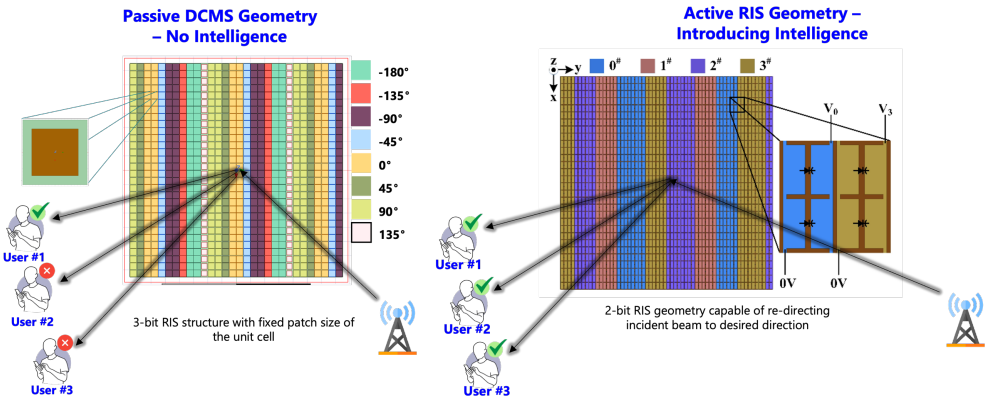

(i) (ii)

Fig.4.1 Comparison of passive DCMS and active RIS architecture (i) Passive DCMS geometry with fixed beam steering (no intelligence), (ii) Active RIS geometry with programmable beam control enabling multi-user support (intelligence).

This limitation is, where the passive surface reflects the incident wave toward a predetermined direction, making it unsuitable for dynamic wireless environments. In practical scenarios, user locations may vary with time, and a fixed beam direction cannot efficiently support multiple users or adaptive communication requirements. Consequently, passive DCMS lacks real-time

reconfigurability and flexibility, which are essential for next-generation wireless systems as shown in Fig. 4.1 (ii).

To overcome these challenges, this chapter introduces an actively controlled RIS, where the EM response of each unit cell can be dynamically tuned using electronic components. By integrating tunable elements such as p-i-n diodes and varactor diodes, the reflection phase of individual unit cells can be adjusted through external biasing. This enables real-time control of the phase distribution across the surface, allowing dynamic beam steering toward different users as required.

The working principle of such electronically controlled elements is discussed in the coming section, followed by the design and implementation of the proposed active RIS. By enabling independent control of unit cells, the proposed approach significantly enhances beamforming flexibility, supports multi-user communication, and overcomes the inherent limitations of passive metasurfaces.

4.2 Working Principle of Electronic Diodes –

To enable dynamic control in the proposed RIS, electronically tunable components such as p-i-n diodes and varactor diodes are incorporated within the unit cell. These components operate based on distinct electrical principles and provide switching and tuning functionalities required for adaptive wavefront control. The equivalent circuit representations of both diodes are illustrated in Fig. 4.2.

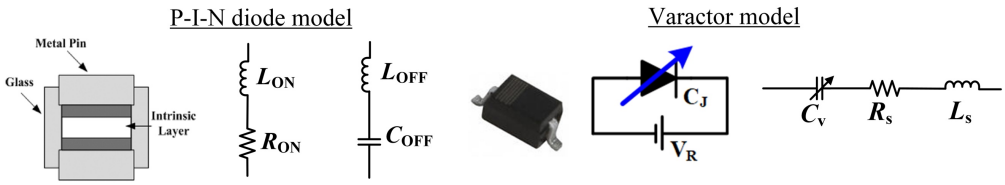

Fig. 4.2 Equivalent circuit models of p-i-n diode in the ON and OFF states and varactor diode illustrating voltage-controlled junction capacitance.

A p-i-n diode operates as a switching element with two discrete states. Under forward bias, it behaves as a low-resistance path, allowing current to flow and effectively connecting different parts of the unit cell. In this ON state, it can be modelled as a small resistance in series with a parasitic inductance. Under reverse bias, the diode presents a high impedance, acting as a capacitive element that blocks current flow. This OFF state can be represented by a capacitance in series with an inductance. The ability to switch between these two states enables rapid transitions between different electromagnetic responses, making the p-i-n diode suitable for controlling discrete functionalities such as reflection or absorption.

In contrast, a varactor diode functions as a voltage-controlled tunable capacitor. When a reverse bias voltage is applied, the depletion region width changes, resulting in a variation of junction capacitance. This capacitance is inversely related to the applied voltage, enabling continuous tuning of the resonant characteristics of the unit cell. By adjusting the bias voltage, the effective capacitance of the varactor can be controlled, which directly influences the reflection phase of the RIS element.

The combined use of p-i-n and varactor diodes provides both discrete switching and continuous tuning capabilities within the same structure. While the p-i-n diode enables state transitions, the varactor allows fine control over the electromagnetic response. This integration transforms the metasurface from a static structure into a dynamically reconfigurable RIS, capable of real-time beam steering and adaptive operation.

4.3 RIS Geometry with Reduced Control Network –

To realize practical reconfigurability with reduced control complexity, a column-wise biased RIS configuration is considered in this section. In this approach, all unit cells within a given column share a common biasing signal, allowing simultaneous control of their electromagnetic response. This significantly simplifies the biasing network compared to fully independent

control, while still enabling dynamic manipulation of the phase distribution across the surface.

By applying different bias voltages to each column, a controllable phase gradient can be established along one direction of the metasurface, which facilitates beam steering. Although this method offers fewer degrees of freedom than fully independent biasing, it provides an effective trade-off between hardware complexity and beamforming capability.

The following subsections describe the unit cell design for the column-wise biased RIS and demonstrate its beam steering performance under different operating conditions.

4.3.1 Unit Cell Geometry –

Continuing from the column-wise biased RIS configuration, the performance of the proposed structure largely depends on the design of its unit cell. The unit cell, shown in Fig. 4.3, consists of a top metallic layer, an FR4 dielectric substrate, an intermediate air spacer, and a copper ground plane. A varactor diode is embedded between two identical rectangular patches on the top layer, with biasing lines connected along the patch edges to enable voltage control. The FR4 substrate has a relative permittivity $\varepsilon_r = 4.4$, $\tan\delta = 0.02$,

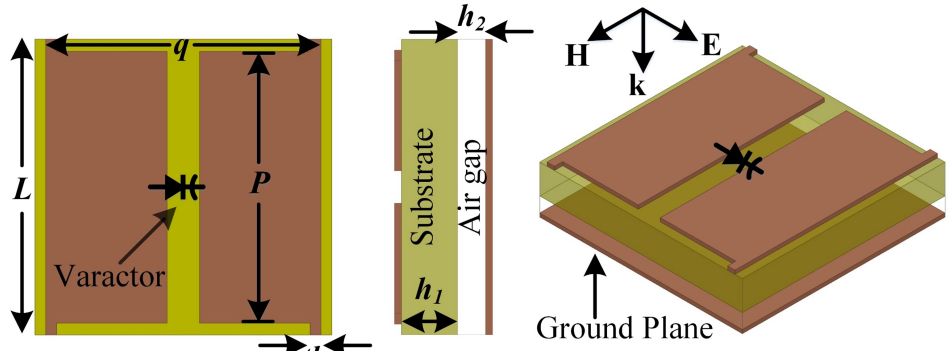

(i) (ii) (iii)

Fig. 4.3 Unit cell geometry of proposed RIS. (i) Top view. (ii) Side view. (iii) Isometric view. The geometric dimensions of the square unit cell are: L = 11mm, P = 10.7 mm, q = 10.8 mm, h_1 = 1.6 mm, h_2 = 0.8 mm, and th = 0.2 mm.

while the ground plane is realized using copper with standard conductivity and thickness.

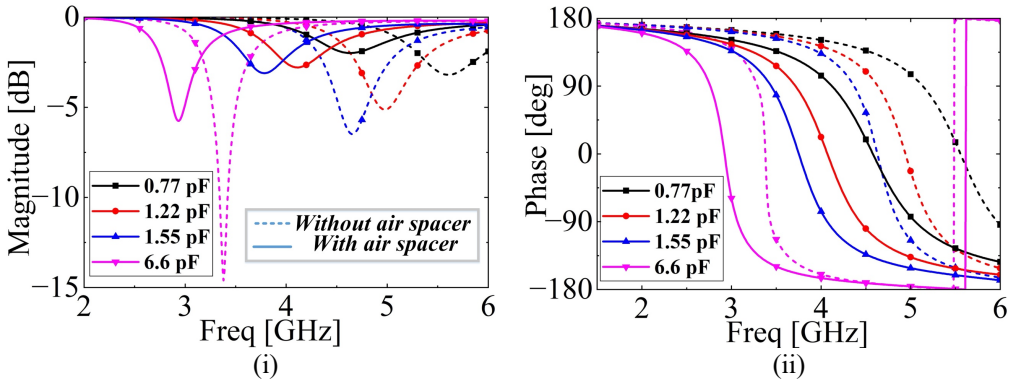

Fig.4.4 Simulated S_{11} responses of the proposed unit cell geometry at four coding states: (i) Magnitude, and (ii) phase states of the proposed RIS with and without air spacer.

The BB857-02 varactor diode is employed to achieve tunability, offering a wide capacitance range from 0.55 pF to 6.6 pF depending on the applied reverse bias voltage. This wide tuning range enables significant variation in the reflection phase, which is essential for RIS operation. However, due to the relatively high loss tangent of FR4, the initial configuration (without an air spacer) results in considerable power dissipation, leading to a degraded reflection magnitude as can be seen in dotted plot in Fig. 4.4 (i).

To mitigate this issue, an air spacer is introduced between the substrate and the ground plane. This modification effectively reduces dielectric losses and improves the reflection performance of the unit cell. As a result, the reflection coefficient magnitude improves significantly as shown in Fig. 4.4 (i), while also maintaining a smooth and wide phase variation as shown in Fig. 4.4(ii). The height of the air gap is optimized to achieve a suitable balance between high reflection magnitude and adequate phase coverage.

The unit cell is simulated using periodic boundary conditions in Ansys HFSS, and its EM response is evaluated by varying the varactor capacitance. Based on this analysis, four discrete phase states are selected to realize a 2-bit coding scheme. These states provide approximately 90° phase separation, enabling effective phase quantization for beam steering. The corresponding

magnitude and phase responses are presented in Fig. 4.4, confirming the suitability of the proposed unit cell for column-wise biased RIS implementation.

The next section presents the beam steering performance achieved using this unit cell configuration under column-wise biasing.

4.3.2 Beam Steering Operation –

The beam steering capability of the proposed column-wise biased RIS is evaluated through full-wave simulations at an operating frequency of 4 GHz. The metasurface consists of an 32×32 array of unit cells, resulting in an overall aperture size of approximately $4.2\lambda_0 \times 4.2\lambda_0$, where λ_0 corresponds to the free-space wavelength at 4 GHz. The structure is excited by a plane wave incident from the far-field region, and the reflection characteristics are analysed by applying appropriate bias voltages across each column to establish the required phase gradient.

Initially, single-beam steering is demonstrated under normal incidence ($\theta_i = 0°$). By introducing a progressive phase variation along the columns, the reflected beam is steered toward a desired angle of $\theta_r = 15°$. The corresponding radiation pattern, shown in Fig. 4.5, confirms that the metasurface successfully redirects the incident wave toward the intended direction. The result validates that even with column-wise control, an effective phase gradient can be realized to achieve accurate beam steering.

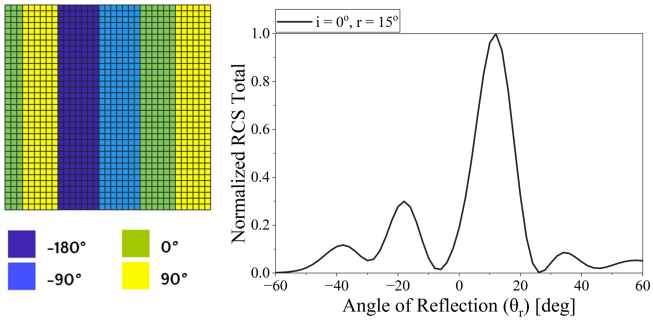

Fig. 4.5 Simulated response of the proposed 2-bit RIS geometry for single beam steering under normal incidence conditions.

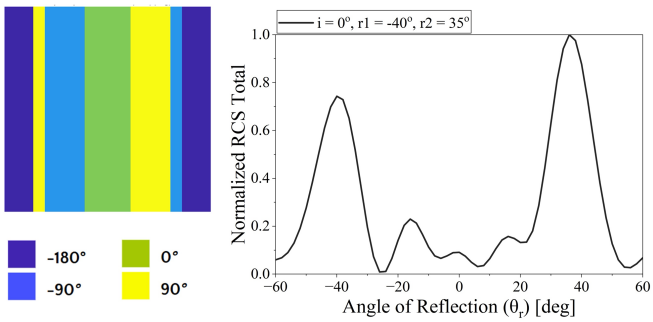

Fig. 4.6 Simulated response of the proposed 2-bit RIS geometry for dual beam steering under normal incidence conditions.

Further, the metasurface is extended to dual-beam operation by synthesizing a combined phase distribution. In this case, the reflected energy is split into two beams directed toward $\theta_{r1} = -40^{\circ}$and $\theta_{r2} = 35^{\circ}$, as illustrated in Fig. 4.6. This is achieved by appropriately assigning coding states across the columns to approximate the superposed phase profile. The simulated radiation pattern confirms the presence of two distinct beams, demonstrating the capability of the proposed structure to support multi-directional coverage.

These results highlight that column-wise biased RIS offers a practical trade-off between control complexity and beamforming performance. While it reduces the number of independent bias lines, it still enables both single and dual-beam steering with reasonable accuracy. Building upon this approach, the next section presents an individually controlled RIS architecture, which provides full control over each unit cell for enhanced beam steering flexibility and multi-user support.

4.4 Individually Controlled RIS Geometry–

While the column-wise biased RIS offers reduced complexity with reasonable beam steering capability, its control is still limited due to shared biasing across each column. To overcome this limitation and achieve maximum flexibility, an individually controlled RIS architecture is considered in this section. In this approach, each unit cell is independently biased, allowing precise control over its reflection phase.

Such independent control enables the realization of arbitrary phase distributions across the metasurface, making it possible to dynamically steer beams in any desired direction, generate multiple beams, and adapt to changing user locations in real time. This significantly enhances spatial resolution, beamforming accuracy, and multi-user support compared to column-wise or passive configurations. However, this improvement comes at the cost of increased biasing complexity and control circuitry.

The following subsection presents the unit cell geometry designed for individually controlled RIS, along with its capability to support independent tuning of each element for advanced beamforming applications.

4.4.1 Unit Cell Geometry –

The individually controlled unit cell, shown in Fig. 4.7, is designed to enable independent phase tuning of each RIS element while maintaining good reflection performance. The top view in Fig. 4.7(i) consists of a copper patch (brown) patterned over an FR4 substrate (green). The geometry includes two rectangular metallic sections, across which a varactor diode is placed. This arrangement introduces inductive behaviour through the narrow metallic strips and capacitive effects due to the gaps around the diode and adjacent patches. An inductor is incorporated along the biasing path to suppress RF leakage into the DC network.

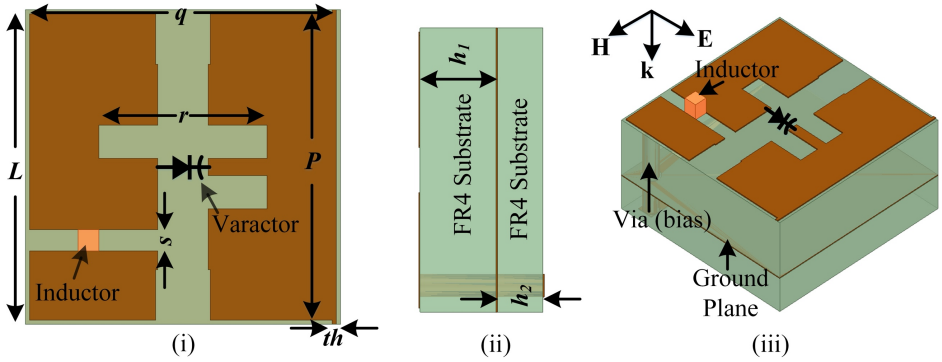

Fig. 4.7 Unit cell geometry of proposed RIS. (i) Top view. (ii) Side view. (iii) Isometric view. The geometric dimensions of the square unit cell are: L = 7.5mm, q = 7.3mm, p = 7.3mm, r = 4mm, s = 0.5mm, h_1 = 2mm, h_2 = 1.2mm, th = 0.1mm.

The side view in Fig. 4.7(ii) shows the multilayer structure, where two FR4 substrates are stacked above a continuous copper ground plane. A metallic via passes vertically from the top patch to the lower biasing layer. Importantly, the via traverses the intermediate region without shorting unintended layers, enabling independent biasing of each unit cell. This via provides the required control voltage to the varactor diode, allowing element-wise tuning of capacitance. The isometric view in Fig. 4.7(iii) illustrates the complete 3D configuration, highlighting the ground plane, dielectric layers, and vertical biasing via, confirming the compact and practical implementation of the structure.

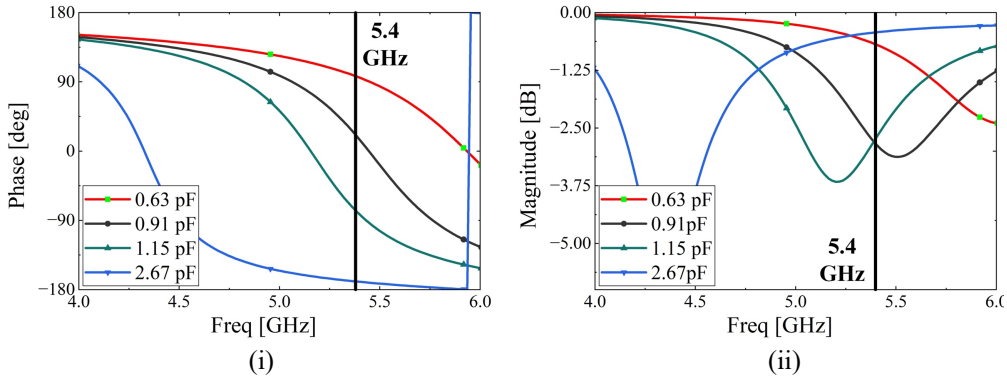

Fig.4.8 Simulated S_{11} responses of the proposed unit cell geometry at four coding states: (i) Phase, and (ii) Magnitude response of the proposed RIS.

The electromagnetic performance of the unit cell is evaluated through its reflection phase and magnitude responses, as shown in Fig. 4.8 (i) and Fig. 4.8 (ii), respectively. By varying the varactor capacitance from 0.63 pF to 2.67 pF, a wide phase tuning range is achieved around the operating frequency of 5.4

Coding States	Capacitance (pF)	Reflection Phase (deg)
#0	2.67	-169
#1	1.15	-79
#2	0.91	11
#3	0.63	101

Table 4.1: Four coding states of the proposed Individually biased RIS.

GHz. Based on this, four discrete capacitance states are selected to realize a 2-bit coding scheme with approximately 90° phase separation between adjacent states as shown in Table 4.1. The reflection magnitude remains better than −3.5

dB at 5.4 GHz for all coding states, indicating acceptable loss performance. These results confirm that the proposed unit cell is capable of providing both sufficient phase coverage and controlled reflection amplitude, making it suitable for individually controlled RIS-based beam steering applications.

4.5 Beam Steering Operation –

Building upon the unit cell design presented in the previous section, the beam steering capability of the individually controlled RIS is investigated in this section. Unlike column-wise biasing, where a group of elements shares the same control, the present architecture enables independent tuning of each unit cell. This allows precise realization of arbitrary phase distributions across the entire aperture, leading to highly accurate wavefront manipulation.

When a plane wave is incident on the metasurface, the desired reflection behaviour is achieved by imposing a spatial phase gradient across the surface. This phase gradient governs the direction of the reflected beam and follows the principle of generalized Snell's law. By appropriately adjusting the bias voltage of each varactor diode, the reflection phase of every unit cell can be independently controlled, enabling dynamic beam steering. Such fine control significantly improves beam accuracy, reduces sidelobe levels (SLL), and enhances flexibility in comparison to previous RIS geometries.

Furthermore, the individually controlled RIS allows extension to multi-beam operation by synthesizing more complex phase distributions. This enables simultaneous communication with multiple users and adaptive beam reconfiguration in real time. In the following subsections, the beam steering performance is demonstrated for both single-beam and dual-beam scenarios, highlighting the advantages of independent element control in advanced RIS-based systems.

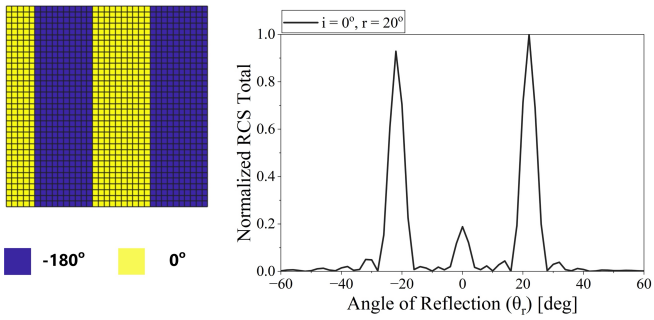

Fig. 4.9 Simulated response of the proposed 1-bit RIS geometry for single beam steering under normal incidence conditions.

4.5.1 Single-Beam Steering –

The single-beam steering mechanism follows the phase gradient principle discussed in Chapter 2 (refer to Eq. 2.1), where the direction of reflection is governed by the imposed spatial phase variation across the metasurface. By assigning appropriate phase states to each unit cell, a linear phase gradient is established, resulting in anomalous reflection toward the desired angle. In the case of the individually controlled RIS, this phase profile is realized with higher precision due to independent tuning of each element, leading to improved beam quality.

Initially, beam steering is demonstrated under normal incidence $\theta_i = 0°$. using a 1-bit coding scheme for a target reflection angle of $\theta_r = 20°$ as shown in Fig, 4.9. The metasurface successfully redirects the incident wave toward the desired direction; however, due to coarse phase quantization, an undesired beam is also observed. This occurs because the limited phase resolution introduces discontinuities in the phase profile, resulting in additional scattering components.

To overcome this limitation, a 2-bit coding scheme is implemented for a higher steering angle of $\theta_r = 45°$ as shown in Fig, 4.10. In this case, four discrete phase states provide a finer approximation of the required phase gradient. The corresponding radiation pattern shows a well-defined main beam directed toward the desired angle with negligible undesired reflections. This

demonstrates that increasing the phase resolution significantly improves beam purity and suppresses spurious lobes.

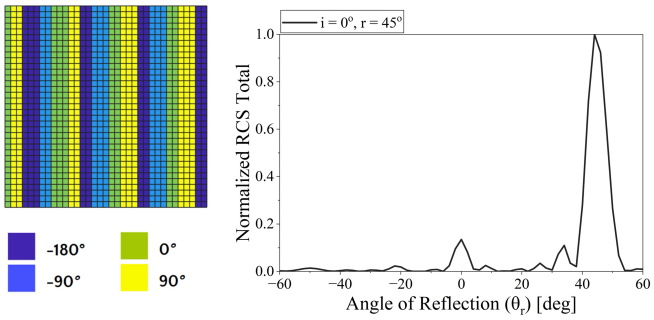

Fig. 4.10 Simulated response of the proposed 2-bit RIS geometry for single beam steering under normal incidence conditions.

Finally, the robustness of the proposed design is validated under oblique incidence conditions. For an incident angle of $\theta_i = 20°$, the metasurface is designed to steer the reflected beam toward $\theta_r = -35°$ as shown in Fig. 4.11. The results confirm that the desired beam direction is accurately achieved even under tilted illumination, indicating good angular stability. This validates the effectiveness of the individually controlled RIS in maintaining reliable beam steering performance under varying incidence conditions.

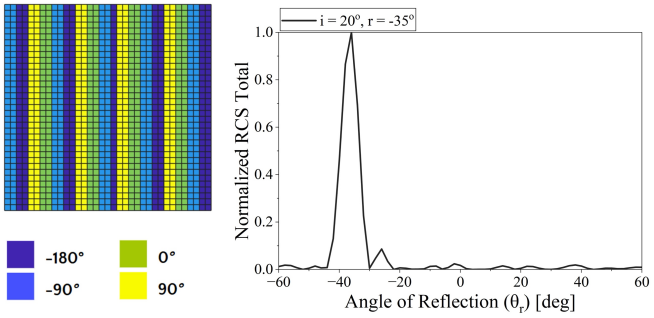

Fig. 4.11 Simulated response of the proposed 2-bit RIS geometry for single beam steering under oblique incidence conditions.

4.5.2 Dual-Beam Steering –

The dual-beam steering mechanism for the individually controlled RIS follows the phase synthesis approach introduced in Chapter 2. By considering two desired reflection angles, θ_{r1} and θ_{r2}, the required phase distributions are

obtained using the formulations given in equation (2.2) and (2.3). These individual phase profiles are then combined using the superposition principle described in equation (2.4), resulting in a composite phase distribution that enables simultaneous generation of two reflected beams. Due to the independent biasing of each unit cell, the proposed RIS can accurately realize this combined phase profile, allowing flexible control over both beam directions and their respective power levels.

In the first case, dual-beam steering is demonstrated using a column-wise biasing configuration, where the phase variation is restricted along one direction ($\phi = 0$). The metasurface is illuminated under normal incidence ($\theta_i = 0°$) and designed to generate two reflected beams at $\theta_{r1} = -15°$and $\theta_{r2} = 30°$ as shown in Fig. 4.12. By appropriately assigning coding states across the columns, unequal power distribution is achieved between the beams, with approximately 20% power directed toward $-15°$and 80% toward 30°. This case highlights that even with limited control (column-wise biasing), the RIS can realize dual-beam functionality with controllable power allocation.

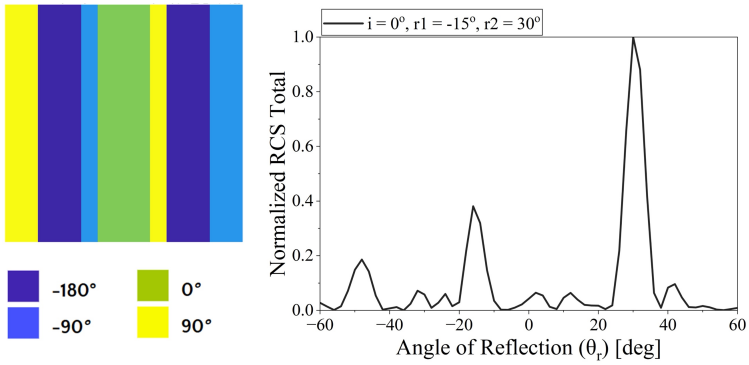

Fig. 4.12 Simulated response of the proposed 2-bit RIS geometry for dual beam steering under normal incidence conditions with unequal power distribution.

In the second case, the full capability of individually biased RIS is utilized. Here, each unit cell is independently controlled in both spatial directions, enabling more advanced beam manipulation. The incident wave is again normal ($\theta_i = 0°$), and two beams are generated at $\theta_{r1} = -15°$with $\phi = 0°$and $\theta_{r2} = 10°$with $\phi = 90°$ as shown in Fig. 4.13. Unlike the previous case, this configuration allows beam steering in both elevation and azimuth planes. The

power distribution is also flexibly controlled, with approximately 70% power directed toward the first beam and 30% toward the second. This demonstrates the key advantage of individually controlled RIS, where independent phase tuning enables multi-dimensional beam steering along with precise power allocation.

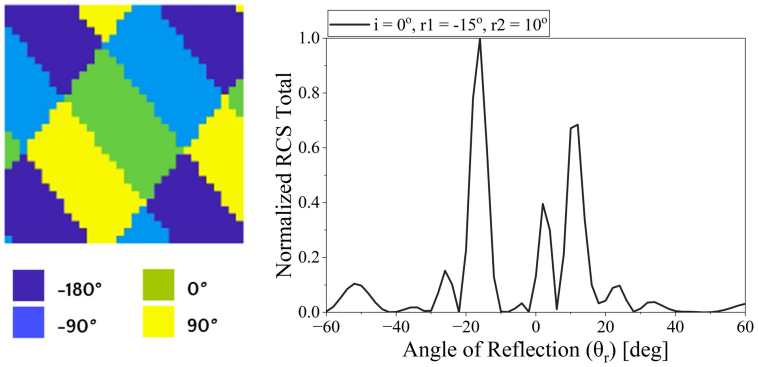

Fig. 4.13 Simulated response of the proposed 2-bit RIS geometry for dual beam steering under normal incidence conditions with unequal power distribution.

Overall, these results confirm that the proposed individually biased RIS provides significantly enhanced flexibility compared to column-wise configurations. It enables accurate realization of dual-beam steering with controllable directions and power distribution, making it suitable for advanced wireless communication scenarios involving multi-user support and spatial multiplexing.

4.6 Conclusion –

In this chapter, an individually controlled RIS has been presented as an advancement over the passive and column-wise biased metasurface designs discussed earlier. The limitations of passive DCMS, particularly the fixed reflection direction after fabrication and restricted support for dynamic user allocation, were addressed through the integration of electronically tunable components. By incorporating varactor diodes within the unit cell, the metasurface is transformed into an adaptive platform capable of real-time control over the reflection characteristics, thereby enabling programmable and reconfigurable beam steering.

The design evolution from column-wise biasing to individually controlled RIS has been systematically demonstrated. Initially, the column-wise biased configuration provided limited phase control along a single dimension, enabling basic single and dual-beam steering operations. However, the introduction of independent biasing for each unit cell significantly increased the available degrees of freedom, allowing precise phase manipulation in both spatial directions. This independent control architecture enabled improved beam steering accuracy, better power allocation between beams, and enhanced adaptability for multi-user scenarios. The proposed unit cell was optimized to ensure stable reflection magnitude and phase performance at the target operating frequency, validating its suitability for RIS-based wireless communication systems.

The key novelty of the proposed geometry lies in its low-cost and practically realizable implementation using an FR4 substrate, which enables easier fabrication and large-scale deployment compared to expensive high-frequency dielectric materials commonly reported in literature. The design is specifically optimized for sub-6 GHz operation, making it suitable for next-generation wireless communication environments where RIS can serve as a cost-effective alternative to conventional phased-array systems. Unlike many reported RIS geometries that neglect practical biasing implementation at the unit-cell level, the proposed design incorporates dedicated biasing vias connected to the control layer for proper voltage regulation of the varactor diodes. Furthermore, the inclusion of lumped inductors along the biasing path effectively suppresses RF leakage into the DC network, thereby improving the reflection magnitude and maintaining stable phase characteristics. This integration of practical biasing architecture with optimized electromagnetic performance highlights the feasibility of the proposed RIS for real-world deployment.

While this chapter focused on achieving programmable beam steering using individually controlled RIS architectures, the following chapter further extends the concept toward multifunctional metasurfaces capable of dynamically switching between RIS operation and microwave absorption. This enables

simultaneous realization of beam steering and radar cross-section reduction functionalities within a single reconfigurable platform.

Chapter 5: Switchable RIS for Dual Functionality

5.1 Introduction –

Metasurfaces enable controlled manipulation of EM waves through engineered amplitude, phase, and polarization responses. This concept has evolved into RIS, where tunable elements such as p-i-n and varactor diodes allow dynamic control of the reflected wave. While conventional RIS designs focus on phase control for beam steering, metasurfaces can also be designed to absorb incident energy, which is important for radar cross-section (RCS) reduction.

To achieve multifunctionality, a switchable RIS is considered, capable of operating in two distinct modes. In one state, the surface acts as a reflective RIS, enabling beam steering through phase tuning. In the other state, it behaves as an absorber, suppressing reflections by dissipating incident energy. However, most existing works address these functionalities separately, and integrating both in a single compact structure remains challenging, especially at sub-6 GHz frequencies.

In this chapter, a switchable metasurface is designed using an FR4 substrate, integrating both p-i-n and varactor diodes within the unit cell. The p-i-n diodes enable switching between reflection and absorption states, while the varactors provide continuous phase tuning for beam steering. This allows simultaneous control of reflection magnitude and phase, enabling dynamic transition between communication and RCS reduction functionalities.

5.2 Reflection and Absorption Mechanism –

The operating principle of the proposed switchable RIS is illustrated in Fig. 5.1. In the OFF state, the surface functions as a reflective RIS, where the incident wave is redirected toward multiple users through controlled beam steering as illustrated in Fig. 5.1 (i). This is achieved by tuning the varactor diodes, which modifies the effective capacitance of the unit cell and provide

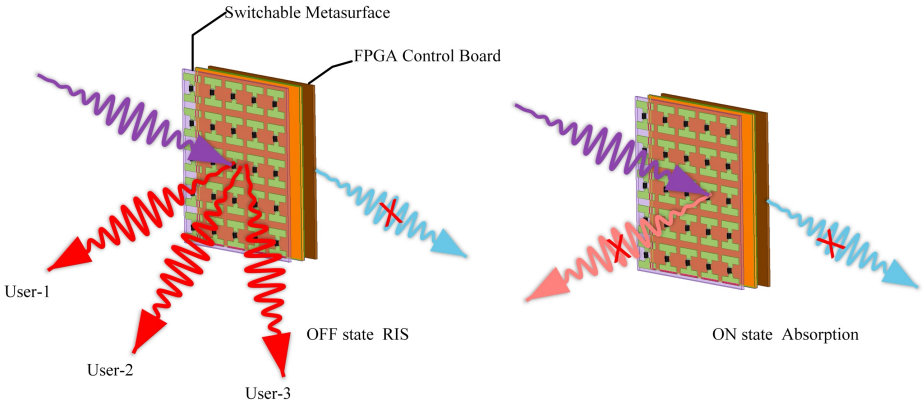

(i) (ii)

Fig.5.1 Schematic representation of the proposed switchable metasurface: (i) RIS reflection for beam steering, (ii) microwave absorber.

the required phase variation. By arranging the phase distribution across the surface, a desired wavefront is synthesized, enabling directional reflection toward specified angles.

In the ON state, the p-i-n diodes are activated, and the structure transitions into an absorption mode. In this condition, the current distribution within the unit cell is altered, introducing higher losses and reducing the reflected energy. The incident wave is largely dissipated within the structure, thereby minimizing reflections as demonstrated in Fig. 5.1 (ii). This behaviour is achieved by designing the unit cell to approach impedance matching with free space in this state, ensuring efficient absorption.

The switching between these two modes is controlled through biasing of the active components. When the p-i-n diodes are OFF, the metasurface maintains high reflection with tunable phase for beam steering. When they are ON, the reflection is suppressed, and the surface behaves as an absorber. As shown in Fig. 5.1, this enables the same structure to either direct energy toward users or reduce its EM signature. This dual functionality makes the proposed RIS suitable for systems requiring both adaptive communication and RCS reduction within a single platform.

5.3 Unit Cell Geometry –

Following the dual-mode operation discussed in the previous section, the unit cell of the proposed switchable RIS is designed to support both reflection and absorption within a single structure. The unit cell consists of a metallic ground plane, two dielectric substrates, and a patterned top metallic layer integrated with active components as shown in Fig, 5.2 (i). The substrates are realized using FR4 with relative permittivity $\varepsilon_r = 4.4$ and loss tangent $\tan \delta = 0.02$, with thicknesses of 3.6 mm and 1.0 mm as shown in Fig. 5.2 (ii). A copper ground plane is used to ensure full reflection, while the top layer comprises rectangular patches embedded with a p-i-n diode, a varactor diode, and an inductor, enabling switching and tuning functionalities. The proposed unit cell geometry is polarization-sensitive due to its asymmetric rectangular patch configuration and biasing arrangement. Consequently, the metasurface is optimized for a single linear polarization, where the incident electric field is aligned with the orientation of the active resonating structure.

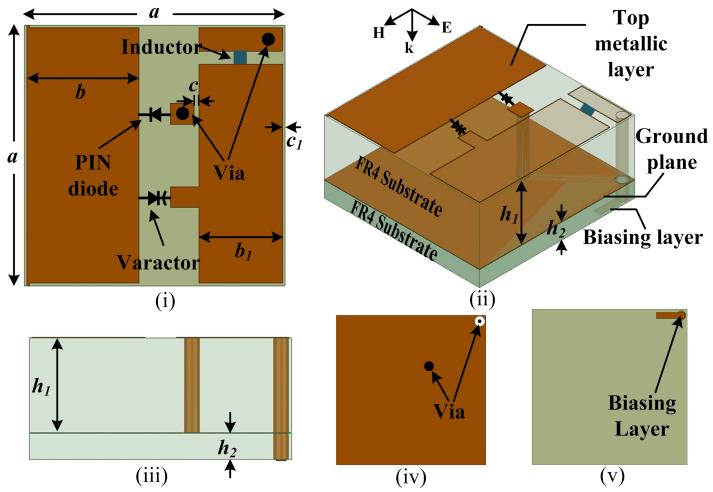

Fig.5.2. Unit cell geometry of the proposed switchable metasurface: (i) Top view, (ii) isometric view, (iii) side view, (iv) ground plane, and (v) biasing layer. The optimized dimensions are as follows: a = 10 mm, b = 4.3 mm, b_1 = 3.2 mm, c = 0.2 mm, c_1 = 0.1 mm, h_1 = 3.6mm, h_2 = 1.0mm.

The electromagnetic behaviour of the unit cell varies with the state of the p-i-n diode. In the ON state, the diode introduces a low-resistance path along with parasitic inductance, increasing losses within the structure. Combined with

substrate losses and biasing effects, this results in strong absorption of the incident wave. In the OFF state, the structure behaves as a reflective RIS, where

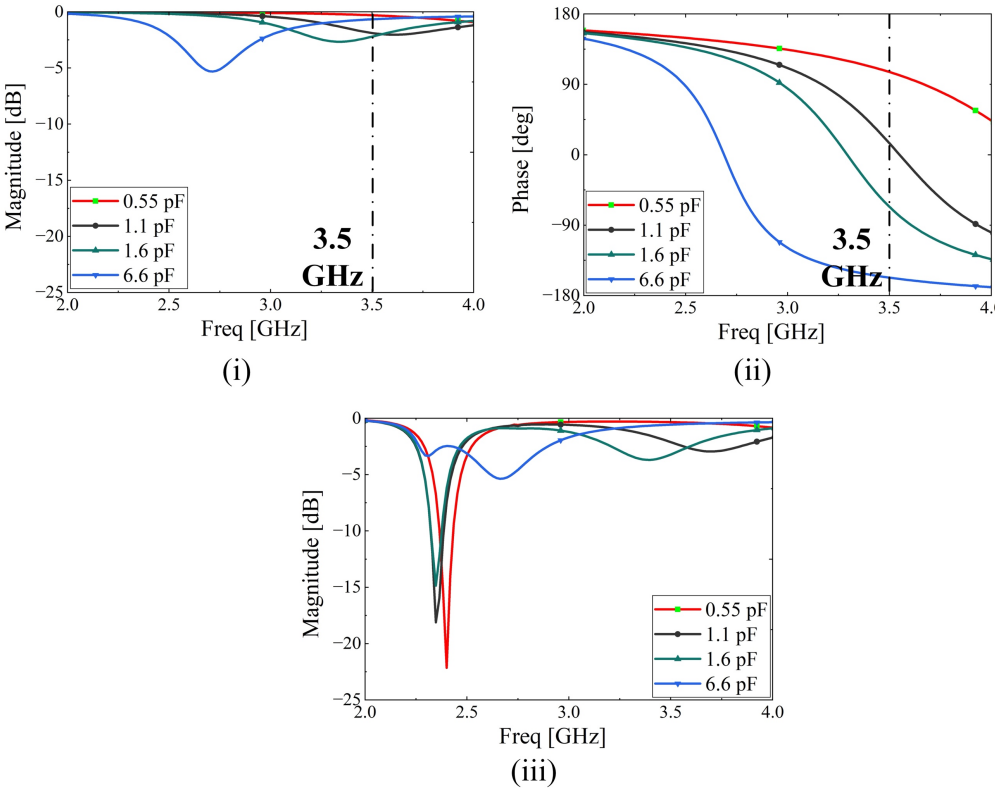

Fig.5.3 Simulation S_{11} response of the proposed switchable metasurfaces under different switching modes. OFF state: (i) magnitude, (ii) phase, ON state: (iii) magnitude.

the varactor diode controls the effective capacitance of the unit cell, enabling phase tuning. Thus, the same geometry supports absorption in one state and controlled reflection in the other, forming the basis of switchable operation.

The varactor diode plays a key role in phase control by providing a wide capacitance tuning range under reverse bias. This enables significant variation in the reflection phase at the operating frequency. However, due to inherent losses from the diode, substrate, and biasing vias, the reflection amplitude tends to degrade. To mitigate this, an inductor is incorporated near the biasing path

Coding States	Capacitance (pF)	Reflection Phase (deg)
#0	6.6	-157
#1	1.6	-67
#2	1.1	23
#3	0.55	113

Table 5.1: Four coding states of the proposed Switchable RIS (OFF State).

to suppress RF leakage, thereby maintaining a high reflection magnitude suitable for RIS operation.

Based on the achievable phase range, a 2-bit coding scheme is implemented, providing four discrete phase states with approximately 90° separation as shown in Table 5.1. These states are obtained by varying the capacitance of the varactor diode through appropriate biasing, enabling controlled phase quantization for beam steering. The unit cell exhibits stable reflection characteristics with acceptable amplitude levels in the reflective state, while in the ON state, it achieves high absorptivity, demonstrating its effectiveness as a switchable RIS for both beam steering and RCS reduction.

5.4 Biasing of Electronic Components –

The biasing network of the proposed switchable metasurface is designed to enable independent control of the p-i-n and varactor diodes while maintaining minimal interference with the RF performance. As illustrated in Fig. 5.4, the p-i-n diode is biased through a vertical via that connects its terminal directly to the intermediate copper layer located beneath the top patch. This configuration allows efficient switching between the ON and OFF states, thereby controlling the transition between absorption and reflective RIS modes. The placement of this via at the central region of the unit cell ensures compact integration without disturbing the surface current distribution significantly.

In contrast, the varactor diode is biased using a separate via that passes across the intermediate copper layer and extends to the bottom side of the unit cell, where the tuning voltage is applied as shown in Fig 5.4. This arrangement enables precise control of the junction capacitance through reverse biasing, which in turn allows continuous tuning of the reflection phase. By isolating the biasing paths of the p-i-n and varactor diodes, the design ensures independent switching and phase control functionalities within the same unit cell.

A column-wise biasing scheme is adopted to provide a common ground reference for both diodes (p-i-n, varactor), simplifying the overall biasing architecture. Additionally, an inductor is incorporated in the biasing path to block RF signals from leaking into the DC network through the vias. This

prevents unwanted power loss and preserves the reflection efficiency of the metasurface. With this biasing configuration, the proposed structure achieves reliable switching and tunability, thereby enabling effective beam steering in the subsequent section.

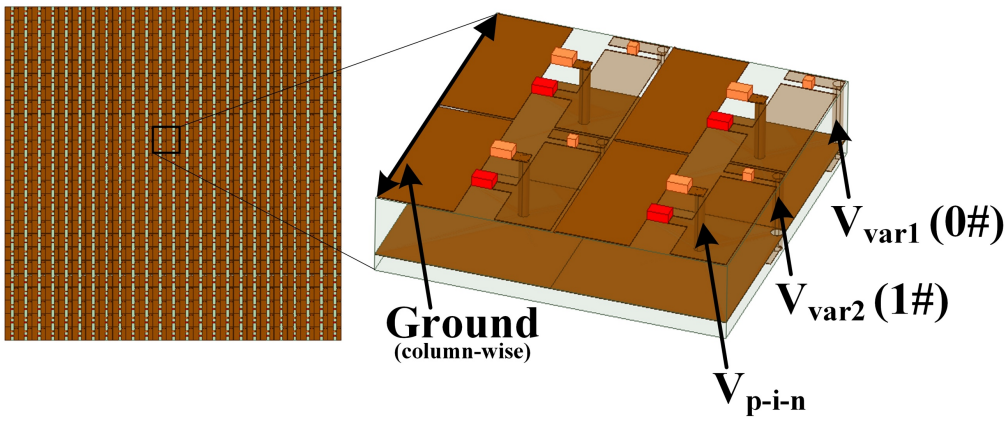

Fig.5.4. Illustration of the biasing present in the proposed switchable metasurface.

5.5 Beam Steering Operation (OFF State) –

Following the biasing configuration discussed in Section 5.4, the proposed metasurface operates in two distinct EM modes depending on the state of the p-i-n diode. When the diode is OFF, the structure behaves as a reconfigurable intelligent surface (RIS), enabling controlled reflection and beam steering. When the diode is ON, the structure transitions to an absorption mode, where the incident electromagnetic energy is dissipated, suppressing reflections. This switchable behaviour allows dynamic control between wavefront manipulation and energy absorption within the same structure.

During RIS operation, beam steering is achieved by introducing a spatial phase gradient across the metasurface. When a plane wave from the far-field impinges on the surface, each unit cell produces a specific reflection phase based on the applied bias to the varactor diode. By arranging these phase states in a progressive manner, a uniform phase gradient is established, enabling anomalous reflection. The relationship between the incident and reflected angles follows the generalized Snell's law, expressed as in eqn 2.1.

The performance of the proposed metasurface is evaluated using full-wave simulations in Ansys HFSS. The structure is excited by a plane wave propagating along the z-axis with the electric field polarized along the y-axis. A finite array of 50×50 unit cells is considered, corresponding to an aperture size of approximately $5.8\lambda_0 \times 5.8\lambda_0$ at the operating frequency of 3.5 GHz. The simulations are carried out for both single-beam and dual-beam steering scenarios under different incidence conditions to validate the effectiveness of the proposed design.

5.5.1 Single-Beam Steering –

The single-beam steering performance of the proposed metasurface is evaluated under different configurations to demonstrate its effectiveness and flexibility. By utilizing the phase gradient formulation described in 2.1, the required reflection direction is achieved through appropriate spatial arrangement of discrete phase states across the aperture.

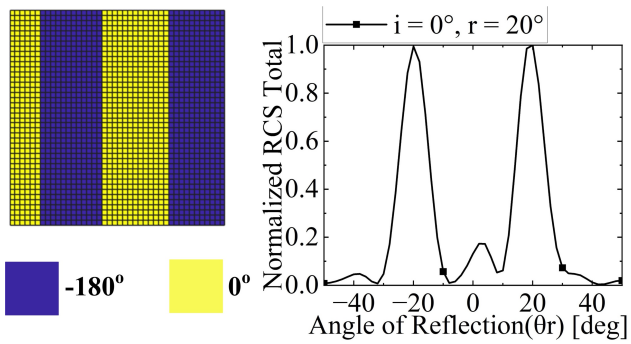

Fig. 5.5 Simulated response of the proposed 1-bit RIS geometry for single beam steering under normal incidence conditions.

Firstly, a 1-bit coding configuration is considered, where two discrete phase states are used to establish the phase gradient. Due to the limited phase resolution, the metasurface produces symmetric beam profiles about the surface normal. This behaviour is evident under normal incidence, where the reflected energy is steered into two symmetric directions, validating the basic anomalous reflection mechanism. The corresponding simulated response is shown in Fig. 5.5, demonstrating the feasibility of beam steering using minimal phase states.

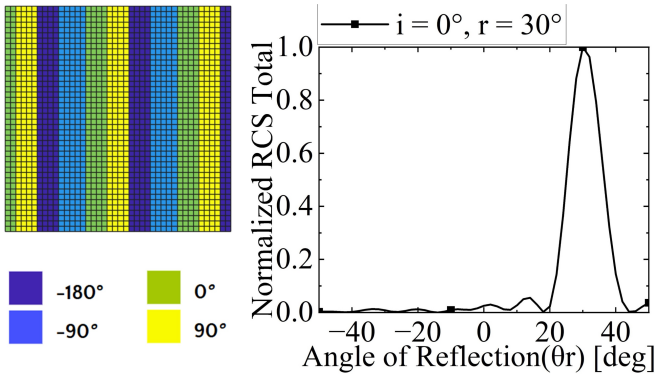

Fig. 5.6 Simulated response of the proposed 2-bit RIS geometry for single beam steering under normal incidence conditions.

Next, the performance is improved by employing a 2-bit coding scheme, which provides four discrete phase states with approximately 90° phase difference between adjacent levels. This increased phase resolution allows a closer approximation of the desired continuous phase profile, resulting in a more focused main beam and reduced sidelobe levels. Under normal incidence, the metasurface successfully redirects the reflected wave toward the intended angle, as illustrated in Fig. 5.6. The improvement in beam quality highlights the advantage of higher phase quantization in achieving efficient wavefront control.

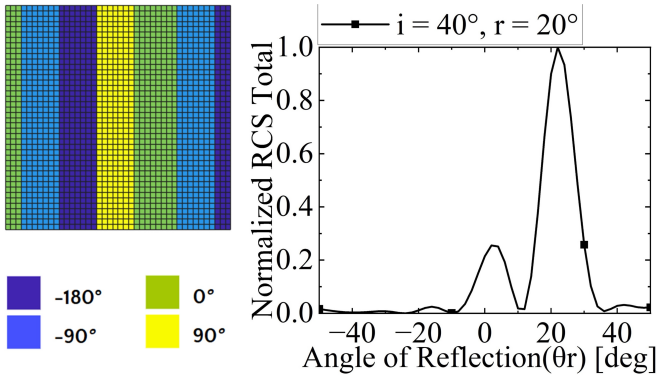

Fig. 5.7 Simulated response of the proposed 2-bit RIS geometry for single beam steering under oblique incidence conditions.

In the final case, the robustness of the design is examined under oblique incidence conditions. Here, the incident wave arrives at a non-zero angle, and the metasurface is designed to redirect the reflected beam toward a specified direction using the same phase synthesis approach. Despite the tilted

illumination, the metasurface maintains the required phase gradient and achieves accurate beam steering, as shown in Fig. 5.7. This confirms good angular stability and demonstrates that the proposed RIS configuration can operate effectively under practical, non-ideal conditions.

5.5.2 Dual-Beam Steering –

The capability of the proposed metasurface is further extended to dual-beam steering by synthesizing a combined phase distribution corresponding to two desired reflection angles. Using the phase profiles defined in eqn. (2.2) and (2.3), and their superposition as expressed in equation (2.4), the metasurface is designed to simultaneously direct the reflected energy toward two distinct directions.

In this configuration, a 2-bit coding scheme is employed to approximate the combined phase distribution using four discrete phase states. The unit cells are arranged based on the synthesized phase profile, enabling the metasurface to split the incident wave into two beams with controlled directions. The simulated radiation pattern, presented in Fig. 5.8, confirms the successful generation of dual beams with good angular separation and balanced power distribution.

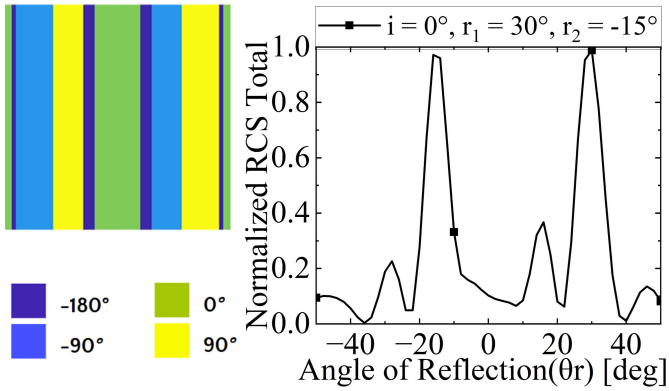

Fig. 5.8 Simulated response of the proposed 2-bit RIS geometry for dual beam steering under normal incidence conditions with equal power distribution.

The results demonstrate that, despite the use of discrete phase states, the metasurface effectively realizes multi-beam functionality with acceptable accuracy. This highlights the capability of the proposed switchable RIS to support multiple users or spatial directions simultaneously during reflective

operation. With both single and dual-beam steering validated, the proposed structure demonstrates its suitability for adaptive electromagnetic applications, leading to absorption or ON State operation of Switchable RIS.

5.6 Absorption Mechanism & RCS Reduction (ON State) –

As discussed in Section 5.5, the proposed metasurface operates as an RIS during the OFF state of the p-i-n diode, where programmable phase control enables beam steering and multi-user communication as shown in Fig. 5.9 (i). In contrast, when the p-i-n diode is switched ON, the metasurface transitions into an absorptive state, where the reflected electromagnetic energy is significantly suppressed. This switching capability enables the structure to dynamically alternate between communication and stealth functionalities depending on system requirements.

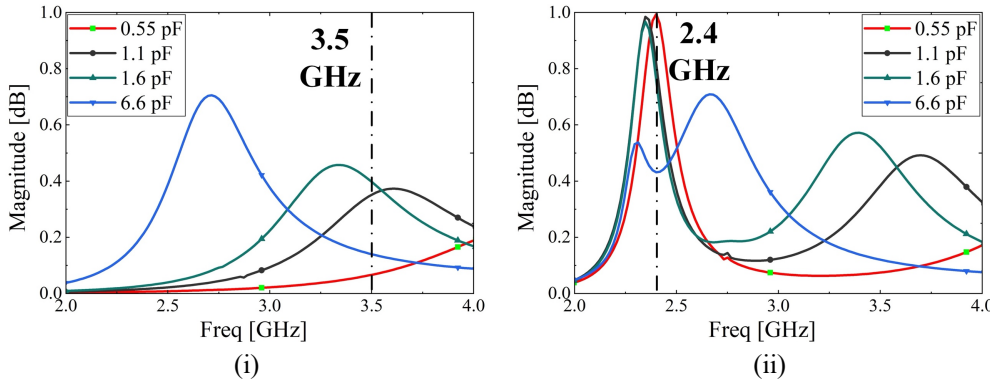

Fig.5.9 Normalized absorption response of the proposed switchable metasurface for different capacitance values: (i) OFF state RIS operation at 3.5GHz, (ii) ON state absorption operation at 2.4GHz

The absorption response of the proposed metasurface in the ON state is shown in Fig. 5.9 (ii). It can be observed that strong absorption occurs near 2.4 GHz for different capacitance values, where the normalized absorption approaches unity. In the ON state, the p-i-n diode behaves as a low-resistance conductive element, allowing stronger surface current flow through the resonant metallic structure. Due to the resistive nature of the diode, dielectric losses of the FR4 substrate, and additional losses introduced by the biasing vias, the incident electromagnetic energy is dissipated inside the structure rather than being reflected back into free space.

The absorption mechanism is primarily based on resonant current excitation within the unit cell. When the incident electromagnetic wave interacts with the metasurface, strong localized currents are generated around the metallic patches, diode region, and biasing paths. Because the p-i-n diode is in the conductive state, these currents experience resistive dissipation, converting part of the incident electromagnetic energy into heat. Simultaneously, the lossy FR4 substrate contributes additional dielectric loss, further reducing the reflected energy. As a result, the reflected wave amplitude decreases significantly, leading to efficient microwave absorption.

This absorption operation is directly related to RCS reduction. In conventional metallic structures, incident radar waves are strongly reflected back toward the source, making the object easily detectable. However, when the proposed metasurface operates in the ON state, the reflected energy is suppressed due to absorption, thereby reducing the backscattered electromagnetic field. Consequently, the apparent electromagnetic signature of the platform is reduced, which is highly beneficial for stealth and low-observable applications.

The integration of RIS and absorber functionalities within a single structure provides significant practical advantages. During normal operation, the metasurface can function as an RIS to establish adaptive wireless communication links through programmable beam steering, improving coverage and signal quality for multiple users. In scenarios where low detectability is required, the same structure can switch to the absorptive state and suppress reflected electromagnetic waves for RCS reduction. Such multifunctional behaviour is particularly useful for aerospace, defence, and next-generation intelligent communication platforms, where simultaneous communication capability and stealth performance are increasingly important.

5.7 Conclusion –

In this chapter, a switchable metasurface has been proposed and analysed to achieve dual EM functionality, namely RIS-based beam steering and microwave absorption. The design integrates p-i-n and varactor diodes within a compact unit cell to enable dynamic switching between reflective and absorptive states. In the OFF state, the metasurface operates as a reconfigurable intelligent surface, providing controllable reflection phase for beam steering. In the ON state, the structure exhibits strong absorption by dissipating the incident electromagnetic energy, thereby suppressing reflections.

The beam steering capability of the proposed metasurface was demonstrated using programmable phase control through varactor tuning. Different coding states were utilized to realize single-beam and dual-beam steering under normal and oblique incidence conditions. The simulated results verified that the proposed RIS can effectively manipulate and redirect the reflected electromagnetic wave toward desired directions. In addition, the ON-state operation exhibited strong microwave absorption near 2.4 GHz, validating the metasurface capability for RCS reduction and stealth applications. Thus, the proposed structure can dynamically switch between communication and absorption functionalities depending on operational requirements.

The key novelty of the proposed design is the use of a low-cost FR4 substrate, enabling simpler fabrication and deployment compared to expensive Rogers-based structures. The metasurface is optimized for sub-6 GHz operation, making it suitable for practical wireless communication systems while simultaneously supporting absorption-based stealth functionality. Another important contribution is the practical biasing architecture integrated within the unit cell. A column-wise grounding scheme is used for both the p-i-n and varactor diodes to simplify the biasing network and reduce unwanted surface current effects. The p-i-n diode is connected to the intermediate copper layer through a dedicated via for switching operation, whereas the varactor diode is independently controlled through a via connected to the bottom biasing

layer. The via passes through the intermediate layer without electrical contact, preventing undesired RF coupling. Furthermore, an inductor is incorporated along the biasing path to block RF leakage into the DC network, thereby improving the reflection magnitude and phase stability of the metasurface.

Overall, the proposed switchable metasurface demonstrates the feasibility of integrating programmable RIS operation and microwave absorption within a single compact platform using a practically realizable biasing architecture. The next chapter presents the overall conclusion and future scope of the thesis.

Chapter 6: Conclusion & Future Scope

6.1 Summary of the Research –

This thesis presents a systematic and progressive exploration of metasurface engineering, beginning with fundamental electromagnetic concepts and advancing toward highly adaptive and multifunctional RIS. The research is structured across various chapters, where each chapter progressively addresses the limitations of earlier designs and introduces improved architectures with enhanced control, flexibility, and real-world applicability. The central theme throughout the work is the evolution from passive and static metasurfaces to fully programmable and dynamically controllable RIS platforms capable of operating in complex electromagnetic environments. Emphasis is placed not only on theoretical understanding but also on practical design considerations such as cost, fabrication feasibility, and scalability, making the proposed solutions relevant for real-world deployment in next-generation communication and defence systems.

Chapter 1 lays the foundation by introducing metasurfaces as artificially engineered, subwavelength periodic structures capable of manipulating electromagnetic waves in ways not achievable with conventional materials. The discussion emphasizes how metasurfaces enable precise control over amplitude, phase, and polarization of incident waves, thereby replacing bulky traditional components with compact planar structures. The transition from conventional reflectors and antennas to metasurface-based solutions is motivated by the growing demand for miniaturization and integration in modern communication systems. This chapter also highlights emerging applications such as intelligent indoor wireless environments, where metasurfaces can be deployed on walls or ceilings to enhance signal coverage, reduce dead zones, and improve link reliability. Additional applications include satellite communication systems, where lightweight and conformal

metasurfaces can replace traditional reflectors, and electromagnetic interference suppression in densely packed electronic systems. By establishing these motivations, **Chapter 1** sets the stage for the need for reconfigurable and intelligent electromagnetic surfaces.

In **Chapter 2**, the theoretical framework governing wave manipulation using metasurfaces is developed in detail. The concept of engineered phase discontinuities is introduced as the key mechanism enabling anomalous reflection and transmission. Generalized Snell's law is presented to describe how a spatially varying phase profile across a surface can redirect EM waves toward arbitrary directions. The chapter further extends this concept to include both single-beam and multi-beam steering by controlling the phase distribution across the metasurface aperture. These formulations provide the mathematical backbone for all subsequent designs in the thesis. The theoretical insights presented here are directly applicable to practical scenarios such as multi-user wireless communication systems, where signals must be steered toward different users dynamically, and advanced radar systems that require precise control over reflected wave. The ability to manipulate wavefronts with high precision also enables applications in imaging systems, sensing, and beamforming networks, reinforcing the importance of this theoretical foundation.

Chapter 3 focuses on the design and analysis of passive DCMS operating at 2.5 GHz. The proposed design demonstrates how discrete phase states can be achieved through geometric variations in the unit cell, enabling beam steering without the use of active components. While the results validate the effectiveness of passive DCMS in redirecting EM waves, a key limitation is identified: the lack of post-fabrication reconfigurability. Once fabricated, the phase distribution and corresponding beam direction remain fixed, restricting the structure to a single predefined functionality. This limitation significantly reduces the adaptability of the metasurface in dynamic environments, where user locations and communication requirements continuously change. As a result, passive DCMS are best suited for static applications such as fixed point-

to-point communication links, radar reflectors with predetermined scattering profiles, and controlled indoor environments with stable user positions. The insights gained in this chapter clearly highlight the necessity for introducing tunability and programmability in metasurface designs to meet the demands of modern adaptive systems.

Design	Unit Cell Dimensions	Operating Frequency	Biasing ability	Beam steering Range	Design Methodology
[1] 	13mm	5 GHz	No bias (Passive)	-60° to 60° [fixed beam steering after fabrication]	1-bit, 2-bit, 3-bit
[2] 	10mm	2.5 GHz	No bias (Passive)	-55° to 55° [fixed beam steering after fabrication]	1-bit, 2-bit, 3-bit
[3] 	7.5mm	5.4 GHz	Individually biased (Active)	-50° to 50° [dynamic beam steering using biasing]	1-bit, 2-bit
[4] 	10mm	3.5 GHz	Individually biased (Active)	-45° to 45° [dynamic beam steering using biasing]	1-bit, 2-bit

Table 6.1 – Comparative overview of the proposed metasurface unit cells across different design stages highlighting unit cells dimensions, operating frequency, biasing capability, beam steering range, and design methodology.

To address the limitations of passive structures, **Chapter 4** introduces active RIS architectures incorporating electronically tunable varactor diodes for dynamic phase control. The chapter first presents a column-wise biased RIS configuration, the concept is further extended to an individually controlled RIS geometry, in which each unit cell is provided with an independent biasing path, enabling precise phase tuning and improved control over the reflected EM wave. The proposed RIS geometries operate at 5.4 GHz, demonstrating single- and dual-beam steering under both normal and oblique incidence conditions. The key novelty of this work lies in the practical biasing architecture integrated directly into the RIS unit cell. Unlike many reported RIS structures that mainly focus on EM response, the proposed designs incorporate dedicated biasing vias connected to the control layer for proper voltage regulation of the varactor diodes. RF choke inductors are also introduced along the biasing paths to suppress RF leakage into the DC network, thereby improving the reflection magnitude and maintaining stable phase characteristics. In addition, the use of

low-cost FR4 substrates instead of expensive Rogers materials enhances fabrication simplicity and scalability for large RIS implementations in the sub-6 GHz region. The proposed architectures provide adaptive beam steering capability suitable for smart wireless communication systems, indoor coverage enhancement, vehicular communication networks, and radar beamforming applications requiring real-time electromagnetic wave control.

Unit Cell Geometry	Magnitude & Phase Plot	Unit Cell Geometry	Magnitude & Phase Plot
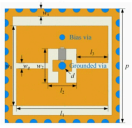 [Ref. (18)]	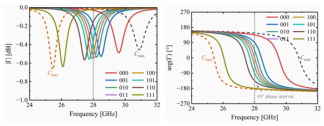 Op. Freq. - 28GHz, Unit Cell Dim. - 3mm, Substrate used - Rogers RO4003C	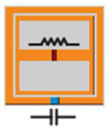 [Ref. (25)]	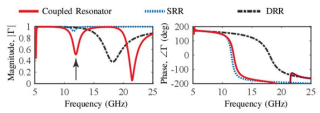 Op. Freq. - 12.5GHz, Unit Cell Dim. - 2.92mm, Substrate used - Rogers RO3006
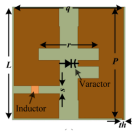 [Design 3]	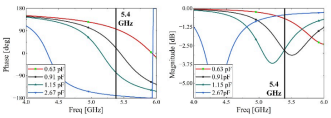 Op. Freq. - 5.4GHz, Unit Cell Dim. - 7.5mm, Substrate used - FR4	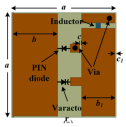 [Design 4]	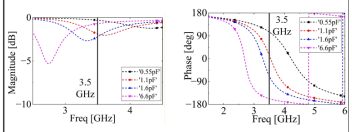 Op. Freq. - 3.5GHz, Unit Cell Dim. - 10mm, Substrate used - FR4
Novelty - The design uses a **low cost FR4 substrate**, enabling easy fabrication and deployment of the proposed RIS geometry. It is optimized for the **sub-6GHz region**, supporting wireless communication applications where RIS can act as a **cost-effective** alternative to **high-cost antennas**.		**Novelty** - The design uses a **low cost FR4 substrate**, enabling easy fabrication compared to Rogers-based structures. It is a switchable RIS with dual functionality, operating for **communication in reflection mode** and as an **absorber for RCS reduction**.	

Table 6.2 – Performance comparison of the proposed RIS unit cells with reported literature, including unit cell geometry, magnitude and phase responses, and highlighting the novelty of low-cost FR4-based designs.

Likewise, **Chapter 5** presents a switchable RIS capable of achieving dual EM functionality, namely programmable beam steering and microwave absorption. The proposed structure integrates both p-i-n and varactor diodes within a single unit cell, enabling dynamic switching between reflective and absorptive operating modes. In the OFF state, the metasurface functions as an RIS, where the varactor diode provides controllable phase tuning for beam steering and wavefront manipulation. In the ON state, the p-i-n diode introduces resistive losses within the structure, allowing the metasurface to operate as a microwave absorber for reflection suppression and RCS reduction. The proposed design operates at 3.5 GHz for RIS functionality and exhibits absorption near 2.4 GHz. A major novelty of this work lies in the integration of a practical biasing architecture within a low-cost FR4-based RIS geometry. Unlike many reported switchable RIS designs, the proposed structure

incorporates dedicated biasing vias, intermediate copper layers, and RF choke inductors to enable reliable control of both p-i-n and varactor diodes while minimizing RF leakage and preserving reflection performance. The use of FR4 substrate also improves fabrication simplicity and scalability compared to expensive Rogers-based structures. The proposed multifunctional RIS is suitable for adaptive wireless communication systems, smart electromagnetic environments, aerospace platforms, and defence applications requiring simultaneous communication capability and stealth performance.

Overall, the research presented in this thesis demonstrates a systematic progression from passive digitally coded metasurfaces to active and multifunctional RIS architectures. In **Chapter 2**, the novelty lies in the formulation and implementation of dual-beam and quad-beam steering using phase superposition principles, enabling simultaneous multi-user wave manipulation through passive DCMS structures. **Chapter 3** extends this concept toward low-frequency RIS operation for SWIPT-enabled IoT applications, where efficient beam steering and energy focusing are achieved using a low-cost metasurface platform. In **Chapter 4**, the proposed individually controlled RIS introduces practical biasing integration using vias, RF choke inductors, and independent varactor control, enabling precise real-time beam steering with enhanced degrees of freedom. Finally, **Chapter 5** presents a multifunctional switchable RIS capable of dynamically operating as both a programmable reflector and a microwave absorber for RCS reduction. The use of low-cost FR4 substrates, practical biasing architectures, and integrated switching mechanisms significantly enhances the feasibility and scalability of the proposed designs for real-world wireless communication, intelligent electromagnetic environments, and stealth applications.

6.2 Scope of Future Work –

While the research presented in this thesis demonstrates significant progress in the design and realization of reconfigurable surfaces - from passive DCMS to multifunctional RIS architectures - several important dimensions remain

open for further exploration and development. The most compelling and immediate direction involves the introduction of true electronic intelligence into the RIS platform through a dedicated control board circuit, thereby completing the transition from a merely reconfigurable surface to a genuinely autonomous and adaptive system as illustrated in Fig. 6.1.

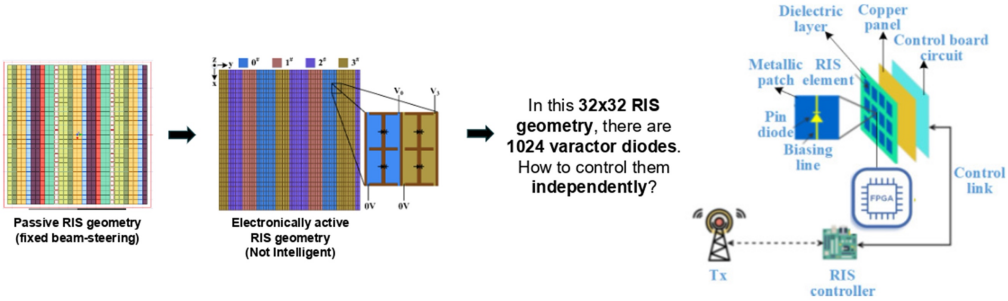

Fig. 6.1 – Evolution from Passive to Electronically Active RIS and Proposed Intelligent Control Architecture for a 32x32 element RIS.

So, moving towards an intelligent RIS, the designs developed in **Chapter 4 & Chapter 5**, particularly the individually biased 32×32 RIS geometry, present a fundamental practical challenge: the surface contains 1024 varactor diodes, each of which ideally requires an independently programmable bias voltage to achieve element-level phase control as demonstrate in Fig. 6.1. Achieving this level of control through conventional static biasing or manual column-wise schemes is neither scalable nor practical in a real-world deployment scenario. The future work therefore proposes the design and integration of a dedicated control board circuit that interfaces directly with the RIS panel, accepts a digital phase pattern as input, and autonomously distributes the correct bias voltage to each varactor diode. This architecture bridges the gap between an electronically active but non-intelligent RIS and a truly programmable, system-aware platform.

The proposed control board circuit, as illustrated in the schematic shown in Fig. 6.2 developed using EasyEDA, is built around three primary functional blocks: a shift-register-based digital input stage, an analog multiplexer (MUX) network, and a PMOS transistor switching layer.

The digital input stage employs serial-in parallel-out (SIPO) shift registers, specifically devices such as the 74HC595 or equivalent. These components receive a continuous bit-stream that encodes the desired phase pattern across the entire RIS aperture. The bit-stream, generated by an upstream controller such as an FPGA or microcontroller, is clocked into the shift registers

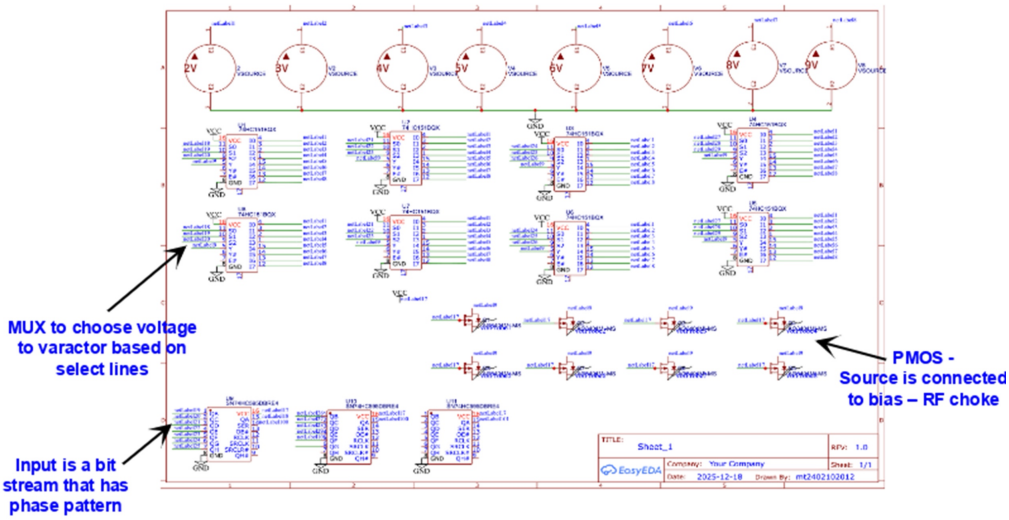

Fig. 6.2 – Schematic of the proposed RIS control board circuit illustrating Shift Register based Digital Input, MUX for Voltage selection, and PMOS based RF-Isolated Biasing Network.

sequentially, after which a latch pulse transfers the stored bit pattern simultaneously to all output lines. This approach dramatically reduces the number of physical control lines needed — instead of routing 1024 separate control wires, only three serial lines (data, clock, and latch) are required, making the design compact and scalable.

The multiplexer network forms the second functional layer. Each MUX receives the digital select lines from the shift register outputs and, based on the binary code presented on those lines, connects one of several pre-set reference voltages to its output. The reference voltages - ranging from 2V through 9V as seen in the schematic - correspond to discrete capacitance states of the varactor diode, and consequently to discrete phase shifts in the reflected electromagnetic wave. For instance, in an 8-state phase configuration, a 3-bit select code from the shift register drives the MUX to route one of eight voltage levels to the corresponding RIS column or element. This design elegantly converts the

digital phase pattern into the analog voltage domain required by the varactor diodes.

The third layer consists of PMOS transistors, whose sources are connected to the selected bias voltage through an RF choke inductor. The RF choke serves a critical dual purpose: it allows DC bias current to pass freely to the varactor diode while presenting a very high impedance to RF signals, thereby preventing the microwave energy on the RIS panel from coupling back into the control circuitry. The PMOS transistor acts as a low-resistance switch that is activated by the corresponding shift register output, completing the bias path to the individual unit cell. The use of PMOS rather than NMOS is deliberate - since the bias voltages are positive and the PMOS source is tied to the supply rail, the gate-low condition needed for turn-on is naturally compatible with active-low logic outputs, simplifying drive requirements.

At the system level, the complete intelligent RIS operates as follows. A transmitter or base station sends a control signal to the RIS controller, which may be a microcontroller or FPGA board. The controller computes the required phase pattern based on the desired beam direction - derived either from a predefined lookup table or from a real-time optimization algorithm such as a codebook-based beamforming scheme. This phase pattern is serialized into a bit-stream and clocked into the shift register chain. Once latched, the MUX network translates each element's digital code into its corresponding analog voltage, and the PMOS switches route these voltages through the RF chokes to the respective varactor diodes on the RIS panel. The entire update cycle can be completed in microseconds, enabling near real-time beam reconfiguration.

This architecture represents a significant step toward practical intelligent RIS deployment, offering full element-level phase programmability, minimal control wiring overhead, compatibility with standard digital logic, and robustness against RF interference in the biasing network. Future work will focus on fabricating and experimentally validating this control board, integrating it with the 32×32 RIS prototype, and evaluating end-to-end system

performance in terms of beam steering accuracy, switching speed, and power consumption — paving the way for deployment in 5G/6G communication testbeds and adaptive radar platforms.

In closing, this thesis has charted a deliberate and rigorous journey through the landscape of metasurface engineering - from the foundational physics of engineered phase discontinuities to the realization of multifunctional, electronically reconfigurable intelligent surfaces. Each stage of the work has been driven by a clear engineering imperative: to build electromagnetic surfaces that are not merely passive reflectors, but active, programmable participants in the communication and sensing environment around them. The proposed future direction of embedding a fully integrated control board circuit into the RIS platform is the natural culmination of this philosophy, transforming the surface from a component into a system. As wireless networks evolve toward 6G and beyond, and as the electromagnetic environment grows increasingly complex and contested, the ability to dynamically shape, redirect, and suppress electromagnetic waves with precision and intelligence will become not a luxury but a necessity. The work presented here lays a concrete and extensible foundation for that future - one unit cell, one phase state, and one programmable surface at a time.

REFERENCES

[1] K. Dautov, G. Nauryzbayev, M. Hashmi, and N. Nasimuddin, "Assessment of compact digital metasurface with beam control for WBAN applications," *51st European Microwave Conference (EuMC)*, London, United Kingdom, 2022.

[2] Elahi M, Jeong T, Yang Y, Lee K-Y, Hwang KC. "A Wideband Reflectarray Antenna for Satellite Application with Low Cross-Polarization." *Applied Sciences*. 2023.

[3] Lin, B., Huang, W., Guo, J., Wang, Z., Si, K., & Zhu, R. (2024). "Ultra-wideband RCS reduction realized by a coding diffusion metasurface." *Journal of Electromagnetic Waves and Applications*, *38*(7), 778–789, 2024.

[4] S. Zhou, T. Li, and E. Li, "Design of resistor-loaded coding metasurface for independent amplitude and phase control," *Journal of Electromagnetic Waves and Applications*, vol. 35, no. 12, pp. 1575–1586, 2021.

[5] B. Ratni, A. de Lustrac, G. P. Piau, and S. N. Burokur, "Active metasurface for reconfigurable reflectors," *Applied Physics Letters*, vol. 124, 2018.

[6] M. Di Renzo, et al., "Smart radio environments empowered by reconfigurable intelligent surfaces: How it works, state of research, and the road ahead," *IEEE Journal on Selected Areas in Communications*, vol. 38, no. 11, pp. 2450–2525, 2020.

[7] J. Yu, W. Jiang, and S. Gong, "Low-RCS beam-steering antenna based on reconfigurable phase gradient metasurface," *IEEE Antennas and Wireless Propagation Letters*, vol. 18, no. 10, pp. 2016–2020, 2019.

[8] R. Malleboina, J. C. Dash, and D. Sarkar, "Design of anomalous reflectors by phase gradient unit cell-based digitally coded metasurface," *IEEE Antennas and Wireless Propagation Letters*, vol. 22, no. 9, pp. 2305–2309, 2023.

[9] K. Singh, M. U. Afzal, and K. P. Esselle, "Accurate optimization technique for phase-gradient metasurfaces used in compact near-field meta-steering systems," *Scientific Reports*, vol. 12, p. 4118, 2022.

[10] Q. Cheng *et al*., "Reconfigurable Intelligent Surfaces: Simplified-Architecture Transmitters—From Theory to Implementations," in *Proceedings of the IEEE*, vol. 110, no. 9, pp. 1266-1289, Sept. 2022 .

[11] X. G. Zhang, D. Pan and W. X. Jiang, "Reconfigurable 2-bit Digital Coding Metasurfaces in a non-contact way," *2018 Cross Strait Quad-Regional Radio Science and Wireless Technology Conference (CSQRWC)*, Xuzhou, China, 2018.

[12] Q. Hu, et al., "Wideband reconfigurable intelligent surface using dual resonance element," *IEEE Antennas and Wireless Propagation Letters*, vol. 22, no. 10, pp. 2422–2426, 2023.

[13] L. Zhang, et al., "Dynamically realizing arbitrary multi-bit programmable phases using a 2-bit time-domain coding metasurface," *IEEE Transactions on Antennas and Propagation*, vol. 68, no. 4, pp. 2984–2992, 2020.

[14] Jianfeng Yang, Juan Chen, Lei Quan, Xiaoming Chen, Hongyu Shi, Wei Xue, and Yajun Liu, "Dynamic radiation steering with transmission-type coding metasurface," *Opt. Express 30*, 28038-28048 (2022).

[15] C. X.Liu et al., "Programmable Manipulations of Terahertz Beams by Transmissive Digital Coding Metasurfaces Based on Liquid Crystals". *Adv. Optical Mater*.2021.

[16] S. Iqbal, et al., "Broadband and high-efficiency manipulation of transmitted vortex beams via ultra-thin multi-bit transmission type coding metasurfaces," *IEEE Access*, vol. 8, pp. 197982–197991, 2020.

[17] J. C. Liang *et al*., "An Angle-Insensitive 3-Bit Reconfigurable Intelligent Surface," in *IEEE Transactions on Antennas and Propagation*, vol. 70, no. 10, pp. 8798-8808, Oct. 2022.

[18] Y. Zhu, et al., "A Varactor-Based Reconfigurable Intelligent Surface Concept for 5G/6G mm-Wave Applications," *2024 18th European Conference on Antennas and Propagation (EuCAP)*, Glasgow, United Kingdom, 2024

[19] S. E. Hosseininejad, et al., "Digital metasurface based on graphene: an application to beam steering in terahertz plasmonic antennas," *IEEE Transactions on Nanotechnology*, vol. 18, pp. 734–746, 2019.

[20] H. Taghvaee, et al., "Scalability analysis of programmable metasurfaces for beam steering," *IEEE Access*, vol. 8, pp. 105320–105334, 2020.

[21] E. Martinez-de-Rioja, et al., "Passive intelligent reflecting surfaces based on reflectarray panels to enhance 5G millimeter-wave coverage," *International Journal of Microwave and Wireless Technologies*, vol. 15, no. 1, pp. 3–14, 2023.

[22] Shahid Iqbal, et al., "Dual-band 2-bit coding metasurface for multifunctional control of both spatial waves and surface waves," *J. Opt. Soc. Am. B* 36, 293-299 (2019).

[23] G. D. Bai, et al., "Multitasking shared aperture enabled with multiband digital coding metasurface," *Advanced Optical Materials*, vol. 6, 2018.

[24] Wang, J., et al., "A Convolution-Based Coding Metasurface for Wide-Angle Beam Steering for Enhanced 5G Wireless Communications". *Materials* 2025.

[25] A. Z. Ashoor and S. Gupta, "Metasurface Reflector with Real-Time Independent Magnitude and Phase Control," *IEEE Transactions on Antennas and Propagation*, vol. 69, no. 5, pp. 2968–2973, May 2021.

[26] A. Samith, R. Zhang, Q. Wu, and C. Yuen, "Intelligent reflecting surface: Practical phase shift model and beamforming optimization," *IEEE Transactions on Communications*, vol. 68, no. 9, pp. 5849–5863, 2020.

[27] W. Long, R. Chen, M. Moretti, W. Zhang, and J. Li, "A promising technology for 6G wireless networks: Intelligent reflecting surface," *Journal of Communications and Information Networks*, vol. 6, no. 1, pp. 1–16, 2021.

[28] M. Ouyang, et al., “Computer vision-aided reconfigurable intelligent surface-based beam tracking: Prototyping and experimental results,” *IEEE Transactions on Wireless Communications*, vol. 22, no. 12, pp. 8681–8693, 2023.

[29] B. G. Kashyap *et al*., "A Reconfigurable Intelligent Surface for 5G Wireless Communication Applications," *2021 IEEE International Symposium on Antennas and Propagation and USNC-URSI Radio Science Meeting (APS/URSI)*, Singapore, Singapore, 2021.

[30] Y. Zhou, L. Chen, Q. Zhang, H. Wang, and L. Guo, “A 1-bit reconfigurable intelligent metasurface-based antenna design for 5G application,” *International Journal of Microwave and Wireless Technologies*, vol. 15, no. 10, pp. 1758–1767, 2023.

[31] W. Li, H. Guo, X. Wang, G. M. Yang, and Y. Q. Jin, “A 2-bit reconfigurable metasurface with real-time control for deflection, diffusion, and polarization,” *IEEE Transactions on Antennas and Propagation*, vol. 72, no. 2, pp. 1521–1531, 2024.

[32] F. Wu, et al., “A 2-bit circularly polarized reconfigurable reflectarray using p-i-n diode tuned crossed-bowtie patch elements,” *IEEE Transactions on Antennas and Propagation*, vol. 71, no. 9, pp. 7299–7309, 2023.

[33] L. Zhang and T. J. Cui, "Angle-Insensitive 2-Bit Programmable Coding Metasurface with Wide Incident Angles," *2019 IEEE Asia-Pacific Microwave Conference (APMC)*, Singapore, 2019.

[34] Q. Hu *et al*., "Design of a Novel 2-bit Wideband Beam-Scanning Reconfigurable Intelligent Surface," *2021 IEEE International Workshop on Electromagnetics: Applications and Student Innovation Competition (iWEM)*, Guangzhou, China, 2021.

[35] Z. Zhang *et al*., "Macromodeling of Reconfigurable Intelligent Surface Based on Microwave Network Theory," in *IEEE Transactions on Antennas and Propagation*, vol. 70, no. 10, pp. 8707-8717, Oct. 2022.

[36] A. Araghi *et al*., "Reconfigurable Intelligent Surface (RIS) in the Sub-6 GHz Band: Design, Implementation, and Real-World Demonstration," in *IEEE Access*, vol. 10, pp. 2646-2655, 2022.

[37] L. Zheng and Y. Zhao, “Generalized snell’s law and its verification by metasurface,” *Proceedings of International Conference on Innovative Mobile and Internet Services in Ubiquitous Computing*, 364–372, Lodz, Poland, July 2020.

[38] Accessed: March 2014. [Online]. Available: https://www.infineon.com/dgdl/Infineon-BB837_BB857SERIES-DS-v01_01en.pdf?fileId=db3a304313d846880113d97339a9011a.

[39] Accessed: December 2020. [Online]. Available: https://www.skyworksinc.com/-/media/5586FCB47A2640488FB7FE939CD86306.pdf

LIST OF PUBLICATIONS

Conferences

1. **Sumit Gaurav**, Patinavalasa Megh Sainadh, Vijay Kumar Sutrakar, Saptarshi Ghosh, "Switchable Metasurface for RCS Reduction and Beam Steering for Aerospace and Defence Systems" – Accepted for Presentation in *IEEE SPACE 2026***,** to be held in Bengaluru, India, 19 - 21 July, 2026.
2. **Sumit Gaurav**, Patinavalasa Megh Sainadh, Okan Yurduseven, Saptarshi Ghosh, "A 3-bit Digitally Coded Metasurface for Beam Steering and SWIPT-Enabled IoT Applications" - submitted in *SPCOM 2026*, to be held in IISc Bengaluru, India, 16 - 18 July, 2026.